Inverse modelling of national and European CH4 emissions using the atmospheric zoom model TM5

P. Bergamaschi, M. Krol, F. Dentener, A. Vermeulen, F. Meinhardt, R. Graul, M. Ramonet, W. Peters, E. J. Dlugokencky

Atmos. Chem. Phys., 5, 2431–2460, 2005
www.atmos-chem-phys.org/acp/5/2431/
SRef-ID: 1680-7324/acp/2005-5-2431
European Geosciences Union

Atmospheric Chemistry and Physics

Inverse modelling of national and European CH_4 emissions using the atmospheric zoom model TM5

P. Bergamaschi[1], **M. Krol**[1,2], **F. Dentener**[1], **A. Vermeulen**[3], **F. Meinhardt**[4], **R. Graul**[4], **M. Ramonet**[5], **W. Peters**[6], **and E. J. Dlugokencky**[6]

[1]European Commission Joint Research Centre, Ispra, Italy
[2]Institute for Marine and Atmospheric Research, Utrecht, Netherlands
[3]Netherlands Energy Research Foundation (ECN), Petten, Netherlands
[4]Umweltbundesamt, Messstelle Schauinsland, Kirchzarten, Germany
[5]Laboratoire des Sciences du Climat et de l'Environment (LSCE), Gif sur Yvette, France
[6]NOAA Climate Monitoring and Diagnostics Laboratory, Boulder, CO, USA

Received: 8 July 2004 – Published in Atmos. Chem. Phys. Discuss.: 25 February 2005
Revised: 30 May 2005 – Accepted: 6 September 2005 – Published: 21 September 2005

Abstract. A synthesis inversion based on the atmospheric zoom model TM5 is used to derive top-down estimates of CH_4 emissions from individual European countries for the year 2001. We employ a model zoom over Europe with $1^\circ \times 1^\circ$ resolution that is two-way nested into the global model domain (with resolution of $6^\circ \times 4^\circ$). This approach ensures consistent boundary conditions for the zoom domain and thus European top-down estimates consistent with global CH_4 observations. The TM5 model, driven by ECMWF analyses, simulates synoptic scale events at most European and global sites fairly well, and the use of high-frequency observations allows exploiting the information content of individual synoptic events. A detailed source attribution is presented for a comprehensive set of 56 monitoring sites, assigning the atmospheric signal to the emissions of individual European countries and larger global regions.

The available observational data put significant constraints on emissions from different regions. Within Europe, in particular several Western European countries are well constrained. The inversion results suggest up to 50–90% higher anthropogenic CH_4 emissions in 2001 for Germany, France and UK compared to reported UNFCCC values (EEA, 2003). A recent revision of the German inventory, however, resulted in an increase of reported CH_4 emissions by 68.5% (EEA, 2004), being now in very good agreement with our top-down estimate. The top-down estimate for Finland is distinctly smaller than the a priori estimate, suggesting much smaller CH_4 emissions from Finnish wetlands than derived from the bottom-up inventory. The EU-15 totals are relatively close to UNFCCC values (within 4–30%) and appear very robust for different inversion scenarios.

Correspondence to: P. Bergamaschi
(peter.bergamaschi@jrc.it)

1 Introduction

Atmospheric CH_4 is the second-most important anthropogenic greenhouse gas (after CO_2) with a direct radiative forcing of $0.48\,Wm^{-2}$ (IPCC, 2001) and an additional indirect forcing of $\sim 0.13\,Wm^{-2}$ due to chemically induced effects (tropospheric ozone and stratospheric water vapor) (Lelieveld et al., 1998). Furthermore, CH_4 has a significant influence on the oxidizing capacity of the atmosphere and hence the lifetime of other trace gases, such as CO, nonmethanehydrocarbons (NMHCs), and hydrochlorofluorocarbons (HCFCs).

General concern about increasing atmospheric levels of greenhouse gases (GHGs) has lead to the United Nations Framework Convention on Climate Change (UNFCCC), which obligates signatory countries to report their annual greenhouse gas emissions, and the Kyoto protocol, which sets legally-binding emission reduction targets for the so-called Annex-1 parties by 2008–2012. The required total reduction of all Kyoto gases together (CO_2, CH_4, N_2O, HFCs, PFCs, and SF_6) for all Annex 1 parties is 5% below the 1990 CO_2 equivalent emissions, while the European Union has committed itself to reduce its total emissions by 8%. Emissions reported to UNFCCC are based on bottom-up inventories, and guidelines for compilation have been elaborated by IPCC (IPCC, 1996). Despite ongoing improvements of these bottom-up inventories, significant uncertainties remain, in particular for some source categories where emission factors may be highly variable (e.g. CH_4 emissions from landfill sites or N_2O emissions from agricultural soils).

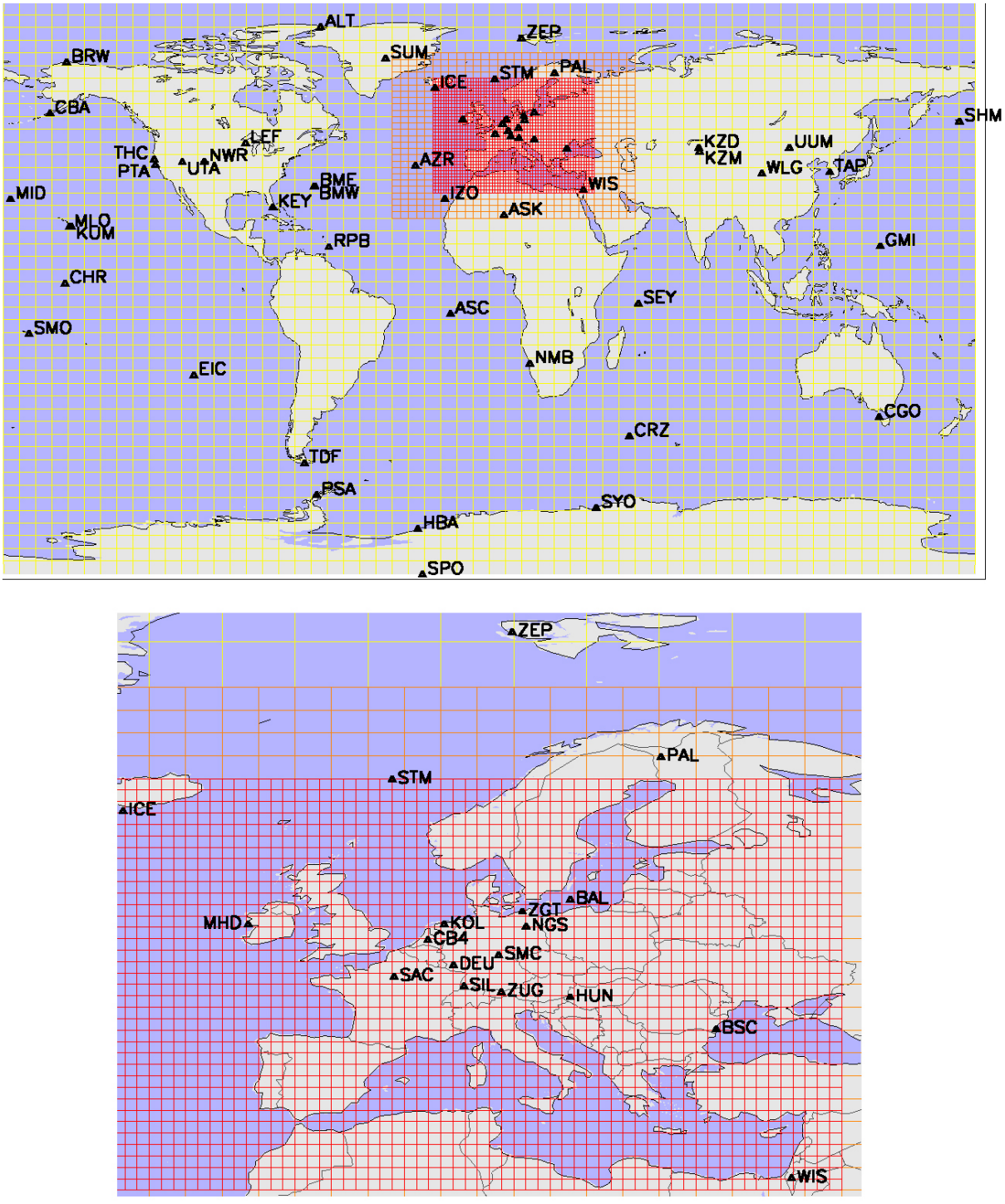

Fig. 1. TM5 grid (6°×4° global grid and 3°×2° and 1°×1° zoom over Europe) and atmospheric CH_4 monitoring sites.

Thus, it is recognized that independent verification of reported national GHG inventories would be very useful (IPCC, 2000). Such a verification could in principle be provided by top-down approaches, based on measurements of atmospheric mixing ratios and inverse modelling.

Inverse techniques have been widely used on the global scale to derive the sources and sinks of the major greenhouse gases CO_2 (Bousquet et al., 1999a, b; Kaminski et al., 1999a, b; Gurney et al., 2002; Rödenbeck et al., 2003), CH_4 (Hein et al., 1997; Houweling et al., 1999; Bergamaschi et al.,

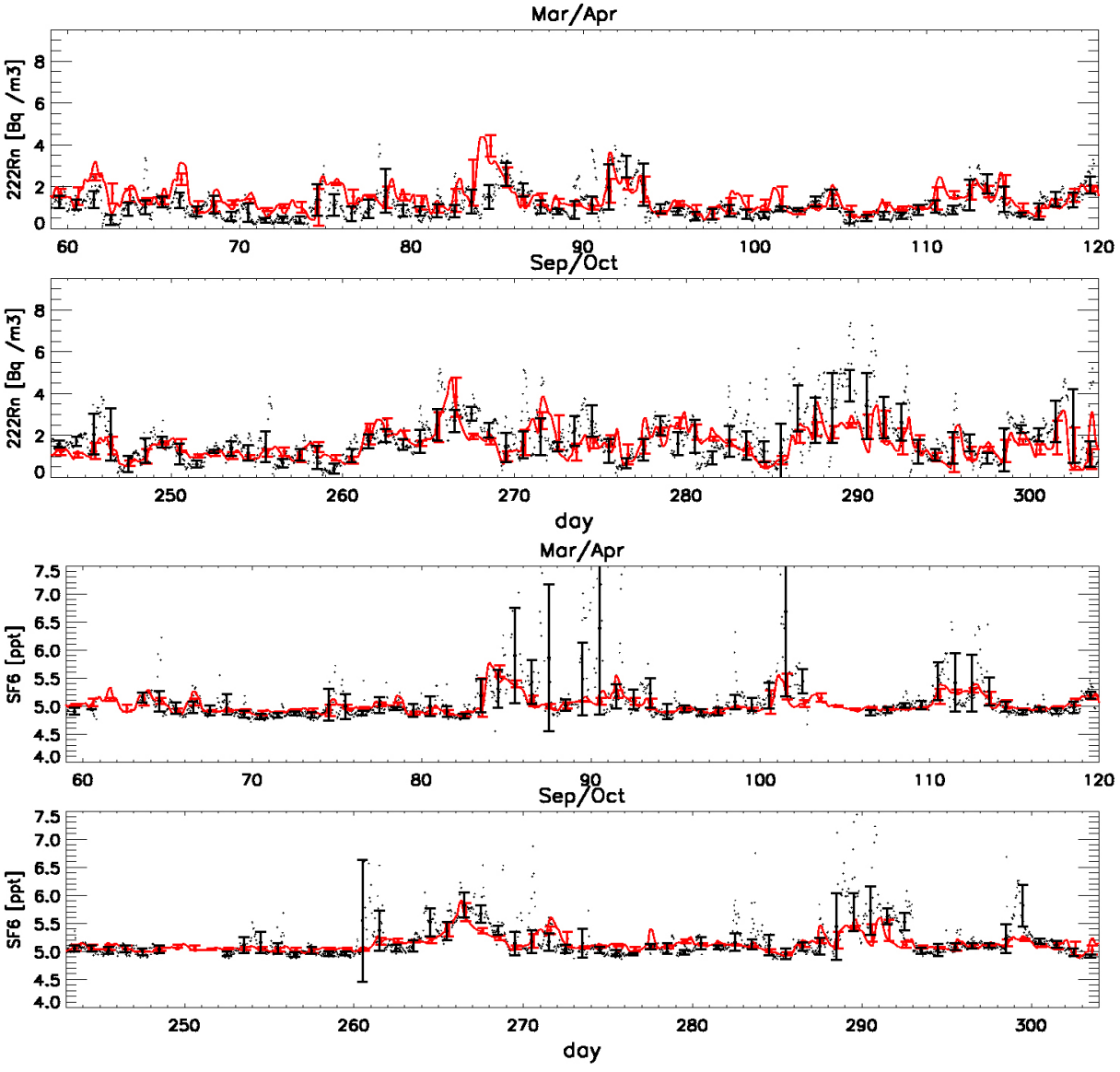

Fig. 2. Station Schauinsland: ^{222}Rn (upper two panels) and SF_6 (lower two panels). Measurements (black) and TM5 model results (red). Bars represent the $\pm 1\sigma$ standard deviation of measurements and model simulations during 24 h.

2000; Dentener et al., 2003a; Mikaloff Fletcher et al., 2004a, b), and N_2O (Prinn et al., 1990). Only during the last few years have attempts been made to derive top-down estimates on national scales, mainly based on Lagrangian back trajectory or Lagrangian particle dispersion models (Vermeulen et al., 1999; Manning et al., 2003). The use of inverse modelling for verification of national bottom-up inventories has recently been discussed at an EU workshop (Bergamaschi et al., 2004).

The global inversions obtained until now generally provide a globally consistent picture; however, they have made little use of synoptic scale variations (usually they use monthly mean values of atmospheric mixing ratios) and provided results only on relatively coarse model grids. In contrast, the studies based on Lagrangian models use short-term variability of meteorological conditions, but are focused on a limited spatial domain (e.g. Europe) and are not, or only weakly, coupled to the global tracer fields.

Here we present an inverse study of European national CH_4 emissions based on the recently developed atmospheric zoom model TM5, which allows us to overcome this scale gap. The zooming approach facilitates – at reasonable CPU costs – consistent high resolution simulations over Europe ($1^\circ \times 1^\circ$), two-way nested into the global model domain (with a resolution of $6^\circ \times 4^\circ$).

Observational constraints are provided by high-frequency (quasi-continuous) measurements of atmospheric CH_4 mixing ratios at several western European monitoring sites (and some global sites), complemented by a comprehensive set of global flask measurements.

2 Inverse modelling setup

2.1 TM5 model

We use TM5, a two-way nested atmospheric zoom model (Berkvens et al., 1999; Krol et al., 2003, 2005). TM5 is an off-line model that uses meteorological fields from the ECMWF IFS model (6-hourly forecast, based on 4D-VAR analyses) (ECMWF, 2002). The global simulations are performed at a horizontal resolution of $6°\times4°$. The embedded European zoom domain is run at a resolution of $1°\times1°$ (Fig. 1), and is surrounded by a somewhat larger $3°\times2°$ zoom region in order to ensure smooth transition between the different domains. We employ the tropospheric standard version of TM5 with 25 vertical layers, which are defined as a subset of the 60 layers of the current ECMWF operational model. About 5 vertical TM5 layers represent the boundary layer (up to $\sim$1 km), 10 the free troposphere, and 10 the stratosphere. Advection is simulated using the slopes advection scheme (Russell and Lerner, 1981). For non resolved vertical transport by deep and shallow cumulus convection the parameterisation of Tiedtke (1987) is used. Vertical turbulent diffusion near the surface has been parameterised according to Holtslag and Moeng (1991), and in the free troposphere the formulation of Louis (1979) is applied. The model transport has been extensively validated using ^{222}Rn, SF_6, and CH_4 (forward simulations), and a detailed comparison with several other models has been performed within the EVERGREEN project (http://www.knmi.nl/evergreen/) (Goede et al., 2002). As an example we show ^{222}Rn and SF_6 simulations and observations from Schauinsland (Fig. 2), illustrating in particular the reasonable simulation of synoptic variations. In addition, an intensive SF_6 validation using a zoom grid over North America has recently been performed (Peters et al., 2004), showing in general good agreement.

Chemical destruction of CH_4 by OH radicals is simulated using pre-calculated OH fields based on CBM-4 chemistry (Houweling et al., 1998) and optimized with methyl chloroform. For the stratosphere, reactions of CH_4 with Cl and $O(^1D)$ radicals are also included, based on the 2-D photochemical Max-Planck-Institute (MPI) model (Bruehl and Crutzen, 1993).

The derived mean tropospheric CH_4 lifetime[1] vs. OH is 9.4 yrs, very close to the Third Assessment Report (TAR) recommended value of 9.6 years (IPCC, 2001).

[1]Defined here as $[CH_4]_{trop}/[dCH_4/dt]^{CH_4+OH}_{trop}$, assuming that the troposphere extends from the surface up to 100 hPa.

2.2 Bottom-up inventories

Bottom-up inventories are used as a priori estimates of emissions. For all anthropogenic sources except rice paddies we use the International Institute for Applied Systems Analysis (IIASA) inventory for the year 2001, based on the Regional Air Pollution Information and Simulation (RAINS) model, which has recently been extended to include greenhouse gases (Klaassen et al., 2004). This inventory reports national annual totals and has been spatially disaggregated on $1°\times1°$ using the EDGAR 3.2 database for the year 1995 (Olivier and Berdowski, 2001). No seasonal variation in emissions is assumed for these sources, except biomass burning, which has been monthly disaggregated as described by Houweling et al. (1999). Monthly mean CH_4 emissions from rice paddies were taken from the Goddard Institute for Space Studies (GISS) data base (Matthews et al., 1991), with their annual total (79.7 Tg CH_4/yr) scaled down to 60 Tg CH_4/yr. Monthly mean natural emissions from wetlands are based on Walter and Heimann (2000) and Walter et al. (2001a, b) and represent a multi-annual average over the years 1982–1993. The original number of 260 Tg/yr from Walter et al. (2001a) has been downscaled in our study to 175 Tg/yr, as Walter et al. (2001a) argue that their value is probably overestimated. Houweling et al. (2000) estimated a pre-industrial wetland source of 130–194 Tg/yr, and it seems likely that the reduction of CH_4 emissions by cultivation and drainage since preindustrial times may have been approximately compensated by the increase of CH_4 emissions induced by the rise of temperature (Walter et al., 2001a). Emissions from wild animals and termites, as well as CH_4 uptake by soils are from the GISS data base (Fung et al., 1991). Emissions from the ocean were provided by Houweling et al. (1999). The bottom-up estimates per region are compiled in Table 1. The global and EU-15 annual totals for the different source categories are summarized in Table 2. Emissions from EU-15 contribute about $\sim$4% of the global total emissions ($\sim$5% of the total anthropogenic emissions). The spatial distribution of CH_4 emissions is shown in Fig. 3. Within the zoom region over Europe the spatial resolution of the emission inventory and of the TM5 model are identical ($1°\times1°$), outside Europe, however, the model is run at $6°\times4°$, i.e. summing up emissions over 24 $1°\times1°$ grid cells.

2.3 Inversion technique

We use the "synthesis-inversion"/Green's function approach (Heimann and Kaminski, 1999; Enting, 2000), describing the total atmospheric CH_4 mixing ratio in space and time $\boldsymbol{d}_{\mathrm{model}}(\boldsymbol{x},t)$ as a linear combination of n_{para} model runs for emissions from different European and global regions and emissions from different months $\boldsymbol{d}_{\mathrm{model},i}(\boldsymbol{x},t)$ (base functions), including one background run (explained

Table 1. Bottom-up emissions per region used as a priori estimates in this study. UNFCCC values (EEA, 2003; 2004) are also listed for EU-15 countries. Furthermore, the results from the inversion (average and range from scenarios S1–S9, and estimated anthropogenic contribution) are summarized. Values are given in Tg CH_4/yr.

	UNFCCC		a priori used in this study			a posteriori		
	[EEA, 2003]	[EEA, 2004]	anthrop.	natural	total	avg S1-S9	range	anthr.
EU-15								
Germany	2.40	4.04	3.62	0.26	3.88±0.64	4.15	(3.90...4.87)	3.89
Italy	1.73	1.68	2.06	−0.04	2.02±0.40	2.15	(2.10...2.19)	2.19
France	3.08	3.01	2.68	−0.11	2.56±0.42	4.43	(3.86...4.71)	4.54
BENELUX	1.49	1.42	1.31	0.15	1.47±0.23	1.60	(1.35...1.67)	1.45
Austria	0.43	0.36	0.33	−0.01	0.32±0.05	0.30	(0.28...0.30)	0.31
Spain	1.92	1.92	1.91	−0.06	1.84±0.32	2.00	(1.96...2.04)	2.06
Portugal	0.51	0.39	0.39	−0.02	0.37±0.08	0.38	(0.38...0.39)	0.40
United Kingdom	2.20	2.19	3.39	−0.04	3.35±0.82	4.21	(3.91...4.40)	4.25
Ireland	0.60	0.60	0.66	−0.01	0.64±0.12	0.34	(0.26...0.75)	0.36
Greece	0.53	0.53	0.42	−0.01	0.40±0.07	0.40	(0.39...0.40)	0.41
Sweden	0.28	0.28	0.22	0.85	1.08±0.44	0.92	(0.86...0.99)	
Finland	0.26	0.26	0.24	2.98	3.23±1.36	0.27	(−0.27...1.30)	
Denmark	0.27	0.28	0.34	−0.01	0.34±0.06	0.33	(0.30...0.34)	0.34
Total EU-15	15.69	16.96	17.59	3.92	21.51±1.92	21.47	(21.05...22.03)	17.55[1] 20.47[2]
Other European								
Switzerland			0.17	−0.01	0.17±0.03	0.19	(0.18...0.20)	
Norway			0.22	0.00	0.22±0.05	0.22	(0.22...0.22)	
North East Europe			5.11	0.65	5.76±1.00	4.28	(4.02...4.63)	
South East Europe			6.84	−0.09	6.75±1.19	4.77	(4.56...5.04)	
Global regions								
Ukraine+Belarus+Moldova			6.72	3.51	10.23±1.90	8.75	(8.60...9.00)	
Alaska+Canada			2.84	6.51	9.35±3.80	10.87	(9.94...11.69)	
USA (without Alaska)			23.68	4.60	28.28±4.27	35.80	(35.01...36.76)	
Tropical America			11.87	8.55	20.41±3.33	25.00	(23.30...27.64)	
South America			25.51	33.62	59.16±11.75	49.02	(42.72...53.86)	
North Africa			19.86	22.53	42.35±8.11	21.07	(15.08...27.70)	
South Africa			18.23	18.70	36.96±7.29	48.71	(44.98...52.28)	
Near East + Central Asia			19.48	1.66	21.15±4.47	18.71	(18.24...19.24)	
Russia			27.87	16.02	43.89±11.36	28.79	(27.14...29.99)	
East Asia			57.15	2.72	59.87±9.79	45.33	(43.30...48.73)	
India + neighbours			63.96	0.55	64.48±10.73	81.57	(75.21...88.33)	
Tropical Asia			31.45	29.06	60.50±11.14	61.75	(54.79...68.22)	
Australia + New Zealand			6.78	8.06	14.84±3.67	10.03	(9.24...10.85)	
Greenland			0.01	0.19	0.20±0.09	0.15	(0.13...0.19)	
Antarctica			0.00	0.00	0.00±0.00	0.00	(0.00...0.00)	
Ocean			2.39	17.17	19.56±8.37	19.56	(not optimized)	
Total			347.73	177.94	525.65±29.63	496.00	(470.41...521.72)	

[1] assuming EU-15 natural sources of 3.92 Tg CH_4/yr
[2] assuming EU-15 natural sources of 1.0 Tg CH_4/yr

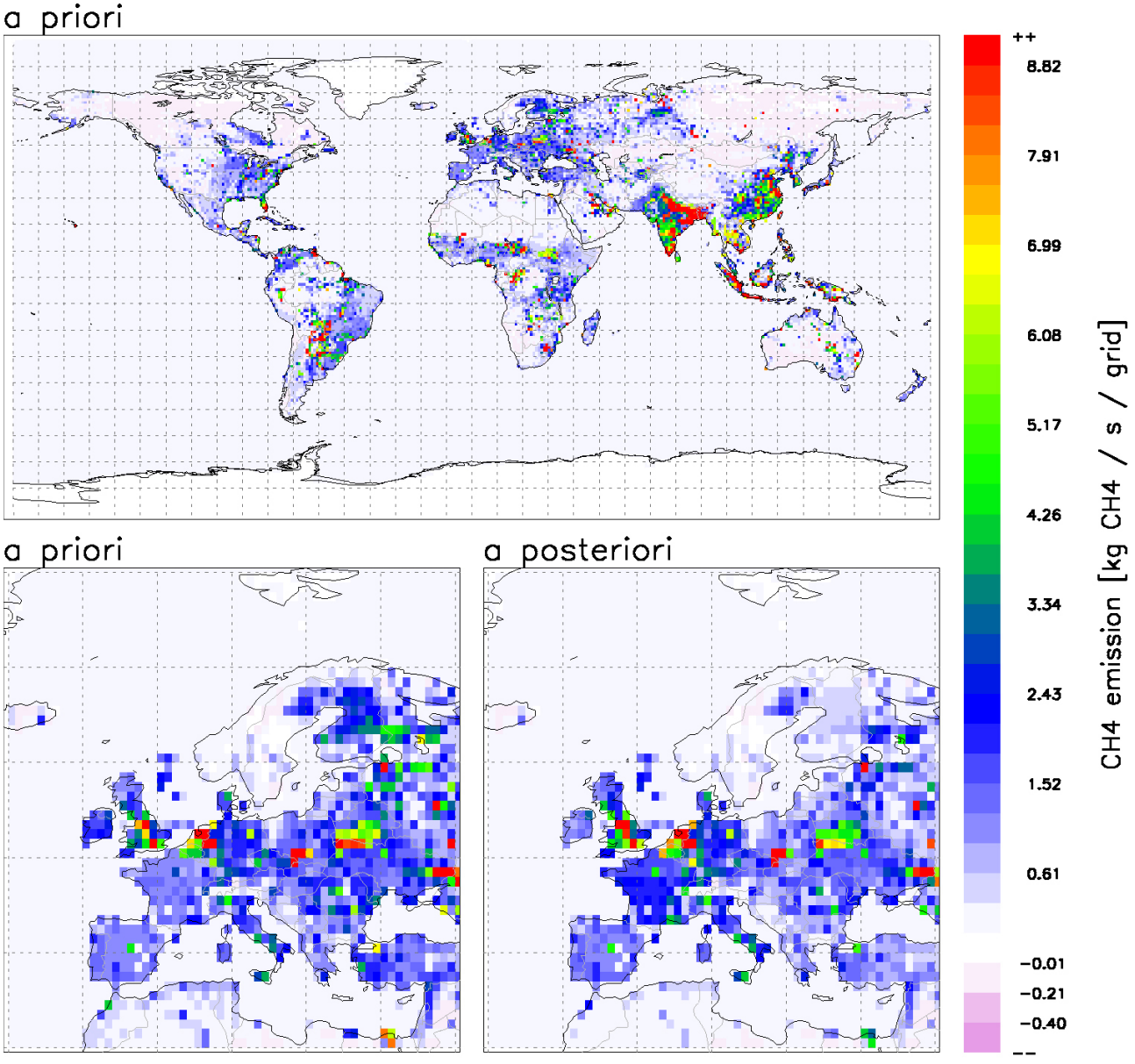

Fig. 3. Spatial distribution of CH_4 emissions. Upper panel shows the global a priori distribution (from bottom-up inventories), and lower left panel the European a priori distribution. Lower right panel shows a posteriori distribution for Europe (average for scenarios S1–S7). Anuual average of total emission per $1°\times1°$ grid cell [kg CH_4/s grid cell].

below):

$$\boldsymbol{d}_{\text{model}}(\boldsymbol{p},\boldsymbol{x},t) = \sum_{i=1}^{n_{\text{para}}} p_i \boldsymbol{d}_{\text{model},i}(\boldsymbol{x},t) \qquad (1)$$

with scaling factors p_i (summarized as vector $\boldsymbol{p}$).

The European domain has been disaggregated into individual countries for all EU-15 countries (except Belgium, Netherlands, and Luxemburg, which are treated as one region (BENELUX)), Norway and Switzerland. Eastern Europe is treated as two separate regions (North East Europe, South East Europe), and all non-European land masses are separated into larger regions (also based on national boundaries, but in most cases combining several countries). The definition of regions is illustrated in Fig. 4. The spatial distribution of countries and their fractional contribution to $1°\times1°$ grid boxes is based on Li (1996).

The temporal disaggregation is performed on a monthly basis, and the individual base functions represent the impact of the emissions from one region and one month. The photochemical sinks (OH, stratospheric $O(^1D)$ and Cl) are included in the base functions directly (in contrast to other

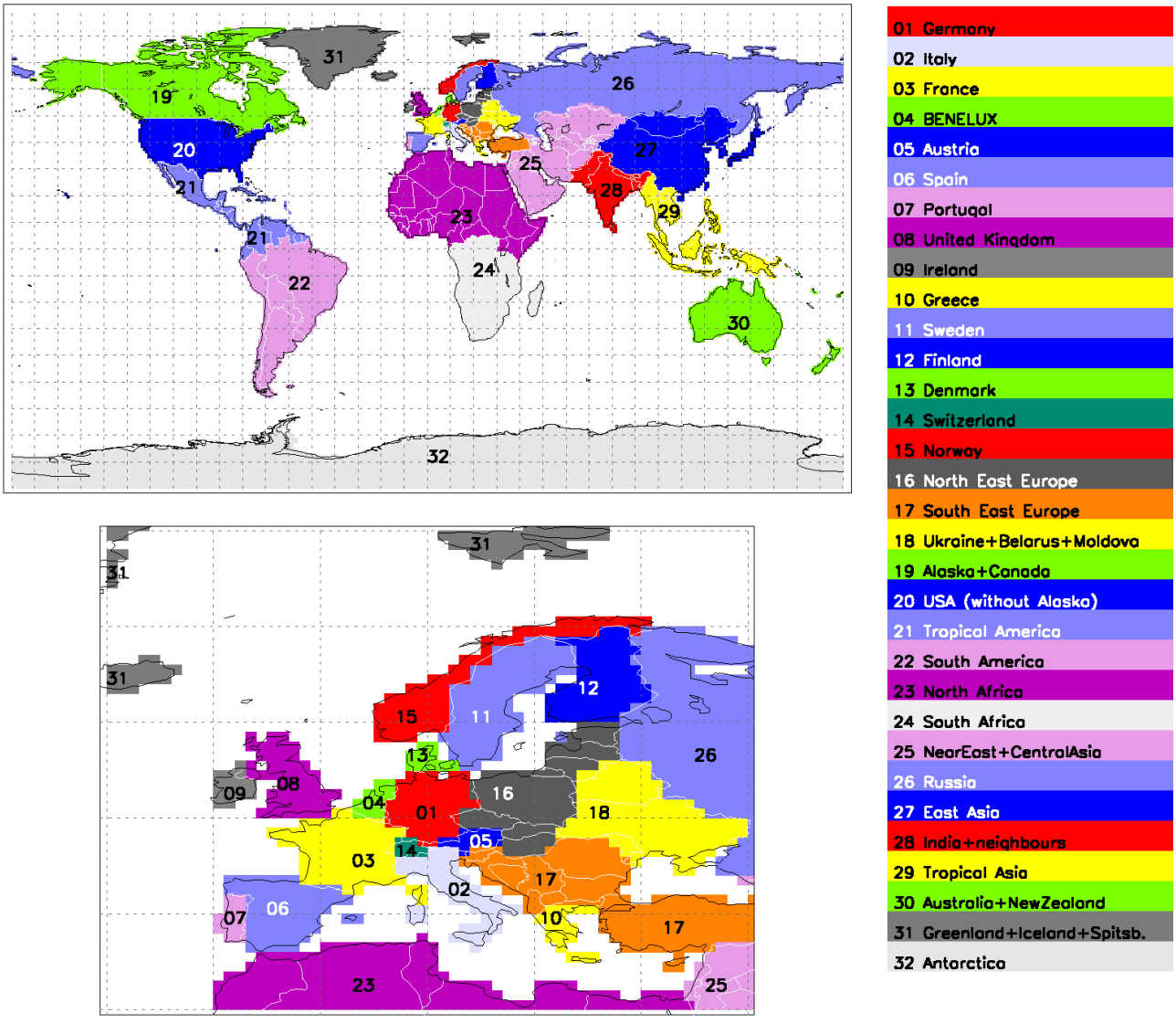

Fig. 4. Global and European regions used for the Green's functions based inversion.

approaches which separate CH_4 sources and sinks; Hein et al., 1997; Houweling et al., 1999).

This study is analyzing the year 2001. Global CH_4 mixing ratios have been initialised using results of a previous inversion. Furthermore, we introduce 2 spin-up months prior to year 2001 (in order to allow some adaptation to potential errors of the initialisation) and simulate also January 2002 (to account for the delayed influence of emissions at monitoring sites). Thus, a total of 2+12+1=15 base functions are calculated for each region. In addition, we calculate one base function for the influence of the model initialization, which accounts for the further development of the initial state of the atmosphere (at 1 November 2000). For this base function, only photochemical sinks are active, but no sources. Consequently, the total number of base functions is n_{para}=(15×33 regions)+1=496. Output of each base function is sampled at hourly intervals, and for comparison with observations averaged to daily mean values.

For the inversion, we follow the Bayesian approach including the a priori knowledge from the bottom-up inventories with the usual definition of the cost function S:

$$S(\boldsymbol{p}) = \langle \boldsymbol{d}_{\mathrm{model}}(\boldsymbol{p}) - \boldsymbol{d}_{\mathrm{data}}, \sigma_{\boldsymbol{d}}^{-1}(\boldsymbol{d}_{\mathrm{model}}(\boldsymbol{p}) - \boldsymbol{d}_{\mathrm{data}})\rangle + \langle \boldsymbol{p} - \boldsymbol{p}_0, \sigma_{\boldsymbol{p}_0}^{-1}(\boldsymbol{p} - \boldsymbol{p}_0)\rangle, \quad (2)$$

where

$\boldsymbol{p}$ is a vector containing all model parameters (i.e. emissions from each region and month, and scaling of background base function); dimension n_{para}

$\boldsymbol{p}_0$ is the a priori estimate of $\boldsymbol{p}$; dimension n_{para}

$\boldsymbol{d}_{\mathrm{data}}$ is a vector containing the observations (daily mean mixing ratios at monitoring sites); dimension n_{data}

Table 2. Global and EU-15 bottom-up emissions per source category in Tg CH_4/yr.

	a priori [Tg CH_4/yr] global	EU-15
anthropogenic sources		
coal	30.7	1.2
oil and gas	50.9	2.0
enteric fermentation	86.3	6.1
manure	14.2	2.0
rice	59.7	0.1
biomass burning	32.3	0.5
waste	73.6	5.7
natural sources		
wetlands	174.5	4.4
wild animals	5.0	0.1
termites	19.2	0.1
ocean	17.0	0.0
total sources	563.4	22.2
soil uptake	−37.8	−0.7
total sources + soil	525.7	21.5

$\boldsymbol{d}_{\text{model}}$ is a vector containing the modelled mixing ratios corresponding to the available observations; dimension n_{data} $\sigma_{\boldsymbol{d}}$ and $\sigma_{\boldsymbol{p}_0}$ are the covariance matrices of the observational data (dimension $n_{\text{data}} \times n_{\text{data}}$) and a priori estimates of the parameters (dimension $n_{\text{para}} \times n_{\text{para}}$), respectively, and $\langle x, y \rangle$ denotes the scalar product. Vectors are identified by Bold Italics, matrices are in Bold Roman.

The minimum of the cost function is calculated according Tarantola and Valette (1982) as:

$$\boldsymbol{p} = \boldsymbol{p}_0 + \left[\mathbf{G}^T \cdot \sigma_{\boldsymbol{d}}^{-1} \cdot \mathbf{G} + \sigma_{\boldsymbol{p}_0}^{-1}\right]^{-1} \cdot \mathbf{G}^T \cdot \sigma_{\boldsymbol{d}}^{-1} \cdot [\boldsymbol{d}_{\text{data}} - \mathbf{G} \cdot \boldsymbol{p}_0] \quad (3)$$

with

$$\mathbf{G}_{ij} = \frac{\partial \boldsymbol{d}_{\text{model},i}}{\partial \boldsymbol{p}_j} \quad (4)$$

and $^{-1}$ denoting the inverse matrix and ^{T} the transposed matrix. The dimension of $\mathbf{G}_{ij}$ is $n_{\text{data}} \times n_{\text{para}}$.

The a posteriori covariance is given as:

$$\sigma_{\boldsymbol{p}} = \left[\mathbf{G}^T \cdot \sigma_d^{-1} \cdot \mathbf{G} + \sigma_{\boldsymbol{p}_0}^{-1}\right]^{-1}. \quad (5)$$

2.3.1 Parameter covariance matrix

For most bottom-up inventories the uncertainties are not specified in detail. Furthermore, correlations of emissions (e.g. of different grid cells or different regions) are usually not known or not specified, which makes a breakdown (or aggregation) of uncertainties for different spatial or temporal scales difficult. In the absence of this information we introduce a simple adhoc approach: We generally assume an uncertainty of 100% per region and per month for each individual source category (for the categories listed in Table 2). An exception is enteric fermentation, for which an uncertainty of 50% per region and month is assumed. Furthermore, we assume a correlation r_{ij} between emissions of two consecutive months as follows:

$$r_{ij} = 0.9 \cdot \frac{e_{\min}}{e_{\max}}, \quad (6)$$

where $e_{\min}$ and $e_{\max}$ are the minimum and maximum monthly emissions of the respective region and source category. Thus for source categories for which no seasonality is assumed, the correlation coefficient for emissions of consecutive months is 0.9, while for sources with seasonality the correlation is smaller. Emissions from different source categories are assumed to be uncorrelated; i.e. the uncertainty of total emissions per region and month is calculated as:

$$\sigma^2 = \sum_{i=1}^{n} \sigma_i^2 \quad (7)$$

(where σ_i are the uncertainties per source category).

Note that the relative contribution from different source categories within individual regions is determined by the a priori inventory only and not further optimized in the inversion.

Emissions of different regions are assumed to be uncorrelated (which is an assumption that is not strictly correct, as in many bottom-up inventories the same underlying assumptions (e.g. emission factors) are used for different countries). The assumed a priori parameter covariance matrix is shown in Fig. 8, with non-diagonal elements only within each region for emissions of different months. Note, however, that the a posteriori covariance matrix shows significant correlations between different regions (as will be further discussed in Sect. 3.2).

Using the correlation coefficients the uncertainty of total emissions per year can be calculated from the monthly uncertainties as:

$$\sigma^2 = \sum_{i=1}^{n} \sum_{j=1}^{n} r_{ij} \sigma_i \sigma_j \quad (8)$$

(i, j: sum over all months; applicable both for a priori and a posteriori uncertainties).

2.3.2 Data covariance matrix

The data covariance matrix $\sigma_{\boldsymbol{d}}$ contains the uncertainties of observations and their correlations. It plays an important role in the inversion, giving high weight to observations with low uncertainty and vice versa.

We generally assume a measurement uncertainty of $\Delta CH_{4\,\text{meas}}$=3 ppb for all data from all sites. However, similar to an approach described by Rödenbeck et al. (2003), we

also include an estimate of the potential model error in the data covariance matrix. We consider the following contributions:

$\Delta CH_{4\,mod1,i}$: The standard deviation between observations and model results of hourly values. This accounts for potential deficiencies of the model to simulate the daily cycle correctly.

$\Delta CH_{4\,mod2,i}$: If not enough hourly observations are available to characterize the diurnal cycle, the standard deviation of hourly model results only is taken instead of $\Delta CH_{4\,mod1}$.

$\Delta CH_{4\,mod3,i}$: To estimate the potential representativeness error, we calculate the spatial gradient of modelled CH_4 mixing ratios at the monitoring sites, using all (horizontally and vertically) adjacent model grid cells. $\Delta CH_{4\,mod3,i}$ is calculated as the daily average of the average gradient in all directions.

The final data uncertainty is calculated as:

$$\left[\Delta CH_{4\,data,i}\right]^2 = \left[\Delta CH_{4\,meas,i}\right]^2 + \left[\max\left(\Delta CH_{4\,mod1/2,i}, \Delta CH_{4\,mod3,i}\right)\right]^2 \quad (9)$$

(index i is used here as data index, i.e. it refers to one particular daily average).

For most NH stations the calculated model uncertainties are typically much larger than the measurement uncertainty $\Delta CH_{4\,meas}$, while high-latitude SH stations are dominated by $\Delta CH_{4\,meas}$.

Due to different temporal resolution of parameters (monthly emissions) and observations (daily mean values), the cost function is strongly biased towards the observations. The dimension of parameter space is n_{para}=496, while typical dimensions of the observation space (e.g. scenario S1, see below) are on the order of $n_{data}\approx$6500. In order to reduce this bias, we introduce a weighting factor for the observations:

$$\left[\Delta CH_{4\,data,i}\right]^2 \rightarrow \frac{1}{\alpha_i}\left[\Delta CH_{4\,data,i}\right]^2 \quad (10)$$

Taking into account the different sampling frequency of continuous measurements (averaged to daily mean values) and flask samples (typically one sample per week), we assign different weighting factors for the two sample types. The default values chosen are $\alpha_{i\,FM}$=1/2 for flask samples and $\alpha_{i\,CM}$=1/6 for daily averages from continuous measurements. The rationale of choosing a ratio of 3 for the weighing factors of the two sampling types is that the timescale for synoptic variations is typically ∼3 days and that air masses originating from the same region(s) contain similar information (i.e. correlated information for different days of particular event). The impact of these weighting factors has been investigated in some sensitivity experiments (see Sect. 3.2.3).

Except for some test experiments (see Sect. 3.2.3), the correlation between observations has been assumed to be zero (i.e. there are only diagonal terms in the data covariance matrix).

2.4 Observations

Observations were used from various networks or groups. Measurement sites are compiled in Table 3. Continuous observations at 5 German sites are from the operational network of the German Umweltbundesamt (UBA). Further continuous European observations have been provided by ECN (at Cabauw (CB4), the Netherlands, which is also part of the CHIOTTO/CARBOEUROPE-IP network), RAMCES/LSCE (at Saclay (SAC), France), the AGAGE network (Mace Head (MHD), Ireland, and further global sites) (Prinn et al., 2000), and the WDCGG data base (at Kollumerwaard, the Netherlands (KOL) and at Izana, Tenerife (IZO)) (WMO, 2003). Furthermore, we use weekly CH_4 measurements from the NOAA/CMDL global cooperative air sampling network (Dlugokencky et al., 1994, 2003) and quasi-continuous measurements from two CMDL observatories at Barrow, Alaska (BRW) and Mauna Loa, Hawaii (MLO) (Dlugokencky et al., 1995) (CMDL data are available from: ftp://ftp.cmdl.noaa.gov/ccg/). We generally apply the NOAA/CMDL CH_4 calibration scale. Observations from the AGAGE network have been converted to the NOAA/CMDL scale by applying a factor of 0.988 (Prinn et al., 2000), and for observations at Kollummerwaard (KOL), which are calibrated versus a NIST standard, a conversion factor of 0.985 has been applied (WMO, 2003). All other observations are already reported versus the NOAA/CMDL scale.

2.4.1 Data selection

Usually the full observational records are used except data which are flagged for technical problems or local contamination. However for a few sites we applied some additional data selection criteria:

At the two mountain sites Schauinsland (SIL) and Zugspitze (ZUG) sometimes upslope winds are observed, in particular during summer daytime. These upslope winds are normally not reproduced by the model, not even on the $1^\circ\times1^\circ$ resolution. Therefore, for these two sites only observations and model results between 20:00 and 09:00 LT are used. The impact of this data selection is investigated in some sensitivity experiments (Sect. 3.2.2).

Furthermore, we apply in some model experiments a data selection for MHD, based on the "pollution flag" provided by AGAGE network.

We generally omit Neuglobsow (NGB) and Trinidad Head (THC) from the inversion, as NGB is very much dominated by regional emissions and model results for THC appear questionable as the corresponding $6^\circ\times4^\circ$ grid cells cover land masses with significant CH_4 emissions and model results are unlikely to represent such coastal site correctly (Peters et al., 2004).

In addition to the abovementioned site-specific selection criteria we generally select outliers, identified by a first iteration of the inversion. All observations which differ from

Table 3. Atmospheric monitoring sites used in this study. "CM" denotes (quasi) continuous measurements, i.e. with a typical time resolution of 1 h or better, and "FM" denotes flask measurements (typical sampling frequency 1/week). The $\Delta CH_{4\,data}$ column gives the average data uncertainty (according to Eq. 9), evaluated for scenario S1. The last columns specify the sites used in the different inversion scenarios.

ID	station name	network	lat. [°]	lon. [°]	alt. [m a.s.l.]	meas. type	$\Delta CH_{4\,data}$ (avg. S1) [ppb]	S1 S5 S6 S8 S9	S2	S3 S7	S4
ALT	Alert, Nunavut, Canada	NOAA/CMDL	82.45	−62.52	210	FM	5.4	x	x	x	x
ZEP	Ny-Alesund, Svalbard, Spitsbergen	NOAA/CMDL	78.90	11.88	474	FM	6.8	x	x	x	x
SUM	Summit, Greenland	NOAA/CMDL	72.58	−38.48	3238	FM	5.4	x	x	x	x
BRW	Barrow, Alaska, USA	NOAA/CMDL	71.32	−156.60	11	CM[1]	12.2	x	x	x	x
PAL	Pallas, Finland	NOAA/CMDL	67.97	24.12	560	FM[3]					
STM	Ocean station M, Norway	NOAA/CMDL	66.00	2.00	7	FM	7.3	x	x	x	x
ICE	Heimay, Vestmannaeyjar, Iceland	NOAA/CMDL	63.25	−20.15	100	FM	10.6	x	x	x	x
BAL	Baltic Sea, Poland	NOAA/CMDL	55.50	16.67	7	FM	14.8	x	x	x	x
CBA	Cold Bay, Alaska, USA	NOAA/CMDL	55.20	−162.72	25	FM	10.8	x	x	x	x
ZGT	Zingst, Germany	UBA/WDCGG	54.44	12.72	1	CM	32.9	x	x		x
KOL	Kollumerwaard, Netherlands	WDCGG	53.33	6.28	0	CM	98.7	x	x		x
MHD	Mace Head, Ireland	AGAGE	53.32	−9.85	30	CM[1]	21.0	x	x	x	x[2]
NGS	Neuglobsow, Germany	UBA/WDCGG	53.14	13.03	65	CM					
SHM	Shemya Island, Alaska, USA	NOAA/CMDL	52.72	174.10	40	FM	7.2	x	x	x	x
CB4	Cabauw, Netherlands, 200.0m	ECN	51.97	4.93	200	CM	53.4	x	x	x	x
DEU	Deusselbach, Germany	UBA/WDCGG	49.76	7.05	480	CM	32.7	x			x
SAC	Saclay, France	RAMCES/LSCE	48.75	2.16	200	CM	37.4	x			x
SIL	Schauinsland, Germany	UBA/WDCGG	47.91	7.91	1205	CM	11.5	x	x	x	x
ZUG	Zugspitze, Germany	UBA/WDCGG	47.42	10.98	2650	CM	9.2	x	x	x	x
HUN	Hegyatsal, Hungary	NOAA/CMDL	46.95	16.65	344	FM	26.5	x	x	x	x
LEF	Park Falls, Wisconsin, USA	NOAA/CMDL	45.93	−90.27	868	FM	13.0	x	x	x	x
KZD	Sary Taukum, Kazakhstan	NOAA/CMDL	44.45	77.57	412	FM	22.3	x	x	x	x
UUM	Ulaan Uul, Mongolia	NOAA/CMDL	44.45	111.10	914	FM	37.8	x	x	x	x
BSC	Black Sea, Constanta, Romania	NOAA/CMDL	44.17	28.68	3	FM	41.9	x	x	x	x
KZM	Plateu Assy, Kazakhstan	NOAA/CMDL	43.25	77.88	2519	FM	15.3	x	x	x	x
THC	Trinidad Head, California	AGAGE	40.80	−124.16	107	CM					
NWR	Niwot Ridge, Colorado, USA	NOAA/CMDL	40.05	−105.58	3475	FM	8.3	x	x	x	x
UTA	Wendover, Utah, USA	NOAA/CMDL	39.90	−113.72	1320	FM	13.2	x	x	x	x
PTA	Point Arena, California, USA	NOAA/CMDL	38.95	−123.73	17	FM	10.9	x	x	x	x
AZR	Terceira Island, Azores, Portugal	NOAA/CMDL	38.77	−27.38	40	FM	5.4	x	x	x	x
TAP	Tae-ahn Peninsula, Republic of Korea	NOAA/CMDL	36.73	126.13	20	FM	33.1	x	x	x	x
WLG	Mt. Waliguan, Peoples Republic of China	NOAA/CMDL	36.29	100.90	3810	FM	17.5	x	x	x	x
BME	St. Davis Head, Bermuda, UK	NOAA/CMDL	32.37	−64.65	30	FM	11.5	x	x	x	x
BMW	Tudor Hill, Bermuda, UK	NOAA/CMDL	32.27	−64.88	30	FM	10.8	x	x	x	x
WIS	Sede Boker, Negev Desert, Israel	NOAA/CMDL	31.13	34.88	400	FM	13.6	x	x	x	x
IZO	Izana, Canary Islands, Spain	WDCGG	28.30	−16.48	2360	CM[1]	9.5	x	x	x	x
MID	Sand Island, Midway, USA	NOAA/CMDL	28.22	−177.37	4	FM	9.8	x	x	x	x
KEY	Key Biscayne, Florida, USA	NOAA/CMDL	25.67	−80.20	3	FM	48.1	x	x	x	x
ASK	Assekrem, Algeria	NOAA/CMDL	23.18	5.42	2728	FM	5.7	x	x	x	x
MLO	Mauna Loa, Hawai, USA	NOAA/CMDL	19.53	−155.58	3397	CM[1]	9.3	x	x	x	x
KUM	Cape Kumukahi, Hawaii, USA	NOAA/CMDL	19.52	−154.82	3	FM	8.5	x	x	x	x
GMI	Mariana Islands, Guam	NOAA/CMDL	13.43	144.78	2	FM	9.4	x	x	x	x
RPB	Ragged Point, Barbados	AGAGE	13.17	−59.43	45	CM[1]	8.9	x	x	x	x
CHR	Christmas Island, Republic of Kiribati	NOAA/CMDL	1.70	−157.17	3	FM	7.9	x	x	x	x
SEY	Mahe Island, Seychelles	NOAA/CMDL	−4.67	55.17	3	FM	14.1	x	x	x	x
ASC	Ascension Island, UK	NOAA/CMDL	−7.92	−14.42	54	FM	6.4	x	x	x	x
SMO	Cape Matatula, Tutuila, American Samoa	AGAGE	−14.23	−170.56	77	CM[1]	7.6	x	x	x	x
NMB	Gobabeb, Namibia	NOAA/CMDL	−23.57	15.03	408	FM	18.1	x	x	x	x
EIC	Easter Island, Chile	NOAA/CMDL	−27.15	−109.45	50	FM	3.3	x	x	x	x
CGO	Cape Grim, Tasmania, Australia	AGAGE	−40.41	144.41	94	CM[1]	8.9	x	x	x	x
CRZ	Crozet Island, France	NOAA/CMDL	−46.45	51.85	120	FM	3.3	x	x	x	x
TDF	Tierra Del Fuego, La Redonda Isla, Argentinia	NOAA/CMDL	−54.87	−68.48	20	FM	3.3	x	x	x	x
PSA	Palmer Station, Antarctica, USA	NOAA/CMDL	−64.92	−64.00	10	FM	3.1	x	x	x	x
SYO	Syowa Station, Antarctica, Japan	NOAA/CMDL	−69.00	39.58	11	FM	3.1	x	x	x	x
HBA	Halley Station, Antarctica, UK	NOAA/CMDL	−75.58	−26.50	10	FM	3.0	x	x	x	x
SPO	South Pole, Antarctica, USA	NOAA/CMDL	−89.98	−24.80	2810	FM	3.0	x	x	x	x

[1] site for which also NOAA/CMDL flask measurements are available (but not not used in our analysis)
[2] model output at virtual site, shifted −2° W and selected observations only
[3] site Pallas: sampling started only end of 2001

model results more than a certain threshold are rejected and not used for the second (final) inversion:

selection criteria:

$$\left|CH_{4\,\mathrm{model},i} - CH_{4\,\mathrm{obs},i}\right| > \lambda \Delta CH_{4\,\mathrm{data},i} \quad (11)$$

with λ=2.

This approach prevents single outliers from introducing a significant bias to the inversion.

The applied threshold to λ=2 leads to a rejection of 12–14% of data points for the scenarios S1–S9 discussed in Sect. 3. Relaxing the threshold to λ=3 strongly reduces the percentage of rejected data to ∼4%, but with an only very small effect on the a posteriori emission estimates.

3 Results and discussion

3.1 Synoptic variability and regional signal

In the following we present the optimized model results along with observations for the European and global monitoring sites. An apparent advantage of the Green's function approach (e.g. compared to 4DVAR techniques) is that it directly provides the attribution of the atmospheric signal to the chosen regions. Figure 5 shows the full year 2001 for Schauinsland (SIL). Figures 6 and 7 show 2 months (September and October 2001) of further European and several global sites, respectively. Plots for the complete year 2001 (similar to Fig. 5) are available for all sites on our ftp server (ftp://ftp.ei.jrc.it/pub/bergamas/CH4BR/). The figures highlight those regions that contribute most to the atmospheric signal (based on the annual average). We define as "direct source contribution" of a certain region the CH_4 emitted in the same month in which the observation has been made plus the CH_4 originating from previous months, weighted with a decay function and a time constant of 31 days. This procedure avoids that CH_4 that was emitted several months ago and "lost its identity" after being cycled over the hemisphere is still attributed to a certain region. The "decayed part" is added to the background (based on the background base function describing the evolution of the initial state of the atmosphere). This total background is displayed in light grey in all figures. The contributions of the remaining regions, which are not among the top 6–10 contributors, are summarized in dark grey ("other"). Hourly observations are shown as black dots, and daily mean values by the black error bars, with the small error bar indicating the 1σ standard deviation of hourly values around the daily mean value, and the large error bar indicating the assigned overall "data uncertainty", including also our estimate of the model uncertainty ($\Delta CH_{4\,\mathrm{data}}$ according to Eq. 9). Grey data points are those which have been rejected by the iterative inversion.

3.1.1 European sites

In general, all European sites are characterized by considerable synoptic variability, i.e. variations due to varying origin of air masses, with typical time scales of a few days. Basing the inversion on daily mean values (instead of monthly means as used for most global inverse studies) directly exploits the information content of these synoptic events in order to derive the emissions from various regions or countries.

A very favourable monitoring site for this purpose is Schauinsland (SIL), located in the Black Forest (South West Germany) at an altitude of 1205 m (Fig. 5). During night-time, the site is usually above the boundary layer and thus dominated by the large-scale influence of Western European CH_4 sources. Some influence of upslope winds during daytime (in particular in summer) from nearby regional sources (mainly from the Rhine valley) has been eliminated in the analysis by selecting only night-time values for the inversion (see also Sects. 2.4.1 and 3.2.2). The strongest direct source signal is from France (13.6 ppb), followed by Germany (8.4 ppb). Further significant European contributions originate from UK (4.5 ppb), BENELUX (2.4 ppb), and Switzerland (2.1 ppb). However, long range transport also plays an important role, particularly from North America (USA (6.8 ppb) and Canada + Alaska (3.3 ppb)), but also from Russia (3.9 ppb) and East Asia (3.4 ppb). As expected, the influence of these more distant regions is much less variable than that of European regions. The seasonal CH_4 cycle appears at this site (as at most other sites with significant direct source influence) mainly in the background, with typical background values of ∼1800 ppb during winter and ∼1750 ppb during summer. The annual average of the total direct source contribution is 65 ppb, however, during individual synoptic events, CH_4 elevations of 150–200 ppb can be reached.

Other European sites are shown in Fig. 6, ordered from North to South. The character of these sites is very different, ranging from sites with very strong total direct source contributions of >100 ppb (Kollumerwaard (KOL), Cabauw (CB4), Deusselbach (DEU), Saclay (SAC), Hegyatsal (HUN), and Black Sea (BSC)) to continental background sites (Zugspitze (ZUG), total direct source contribution 41.7 ppb) and several Atlantic background sites with typical total direct source contributions of 30–40 ppb (Ocean Station M (STM), Heimay (ICE), Terceira Islands (AZR), and Izana (IZO)).

All European sites show a considerable synoptic scale variability and concomitant change of region of influence. In addition, short-term variations of the background are considerable (on the order of 20–30 ppb), particularly visible at sites with small direct source contributions. This confirms the importance of coupling European simulations with a global model.

Some of the European sites (and the majority of global sites) employ only flask sampling, with typical sampling

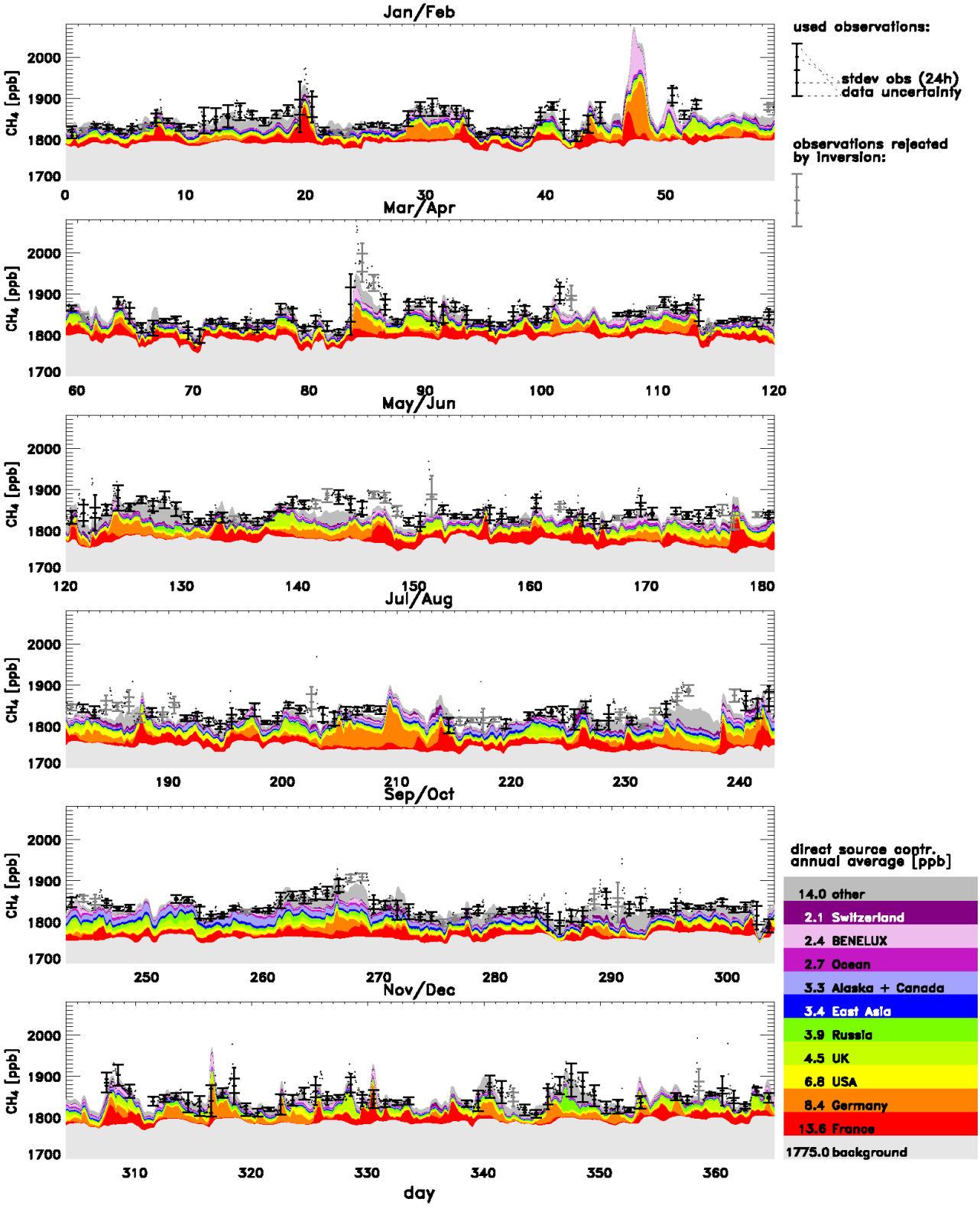

Fig. 5. Monitoring site Schauinsland: Observed and modelled CH_4 mixing ratios for 2001. Colors highlight influence from different regions or countries (see legend and description in Sect. 3.1).

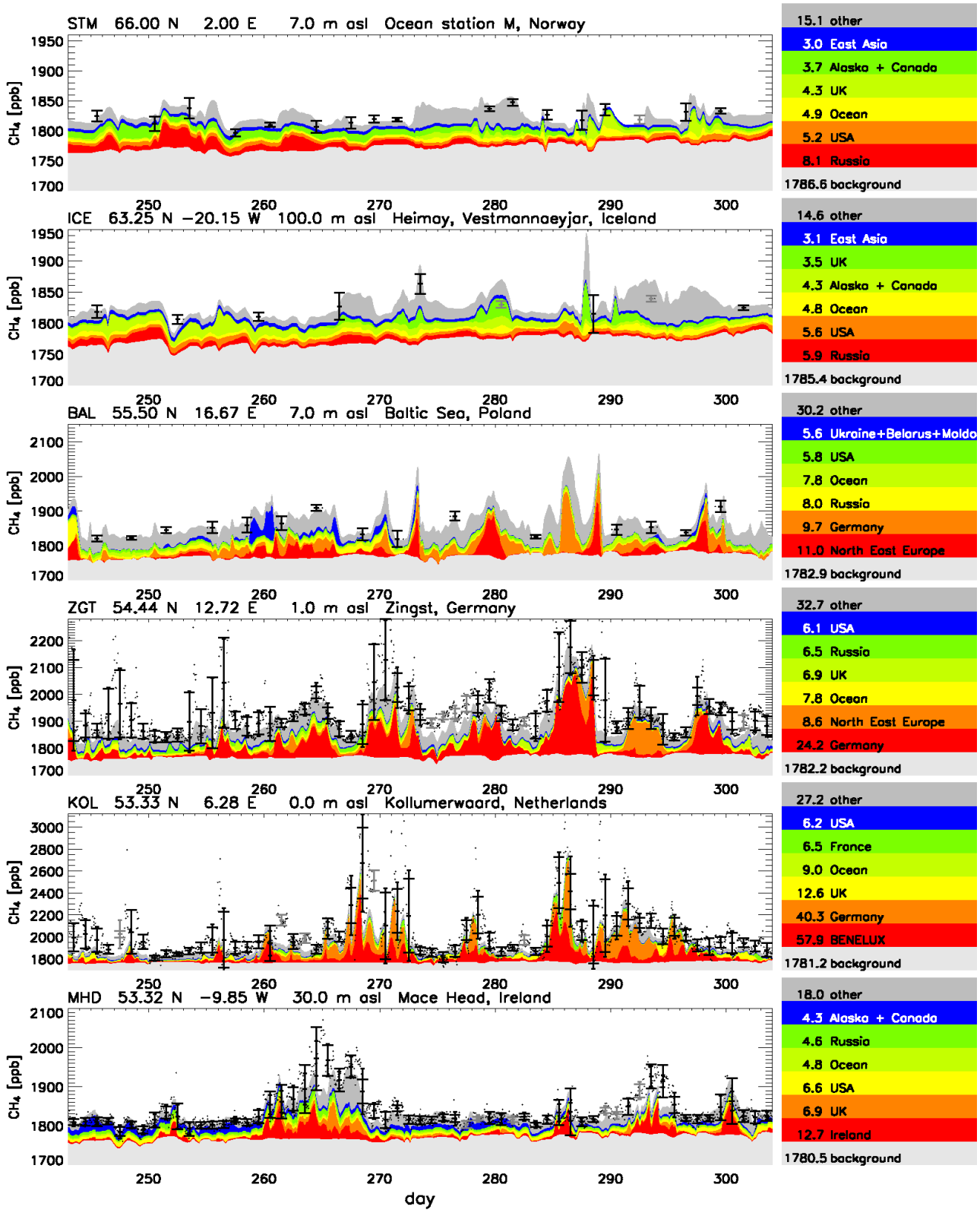

Fig. 6. Observed and modelled CH_4 at European sites for September and October 2001.

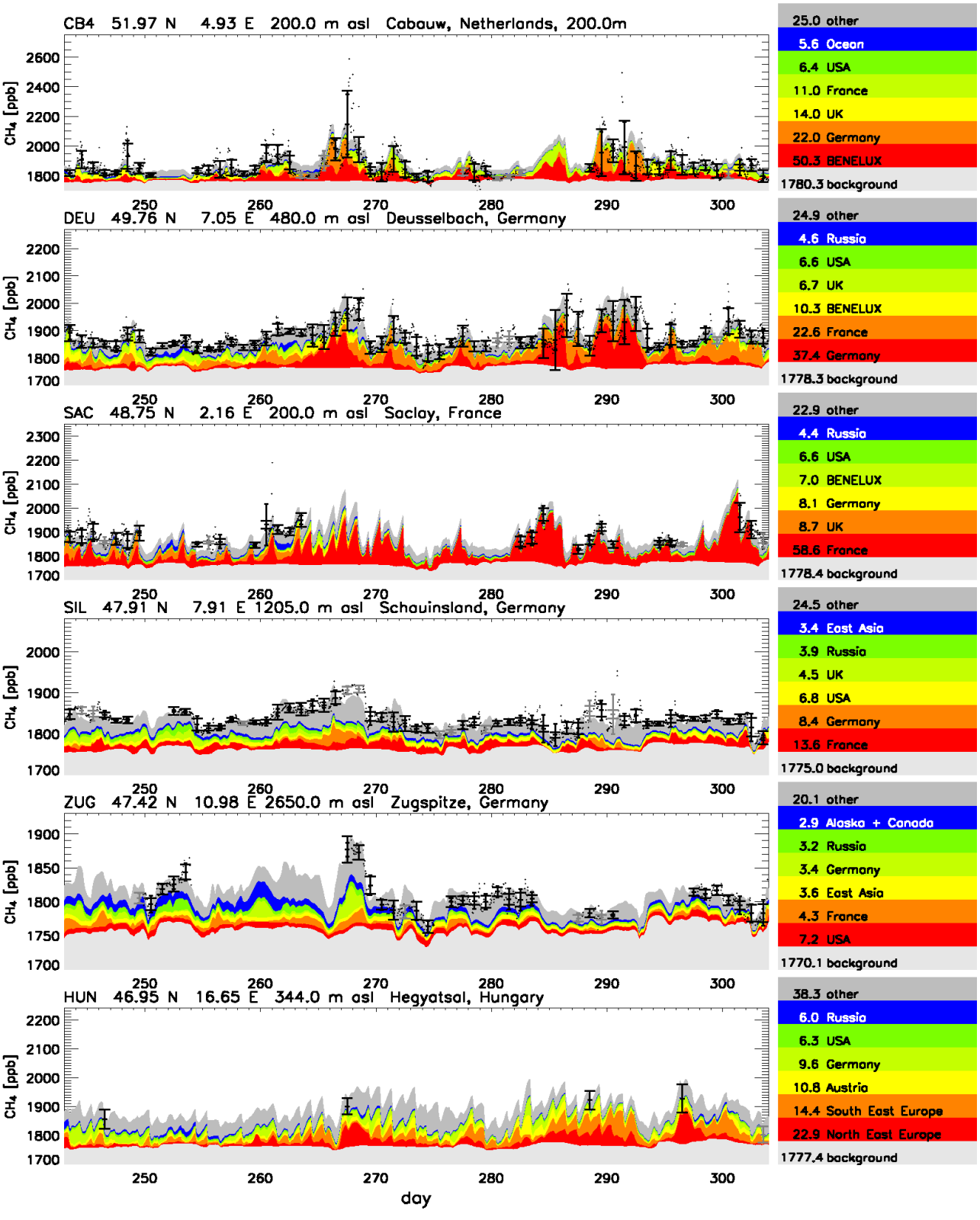

Fig. 6. Continued.

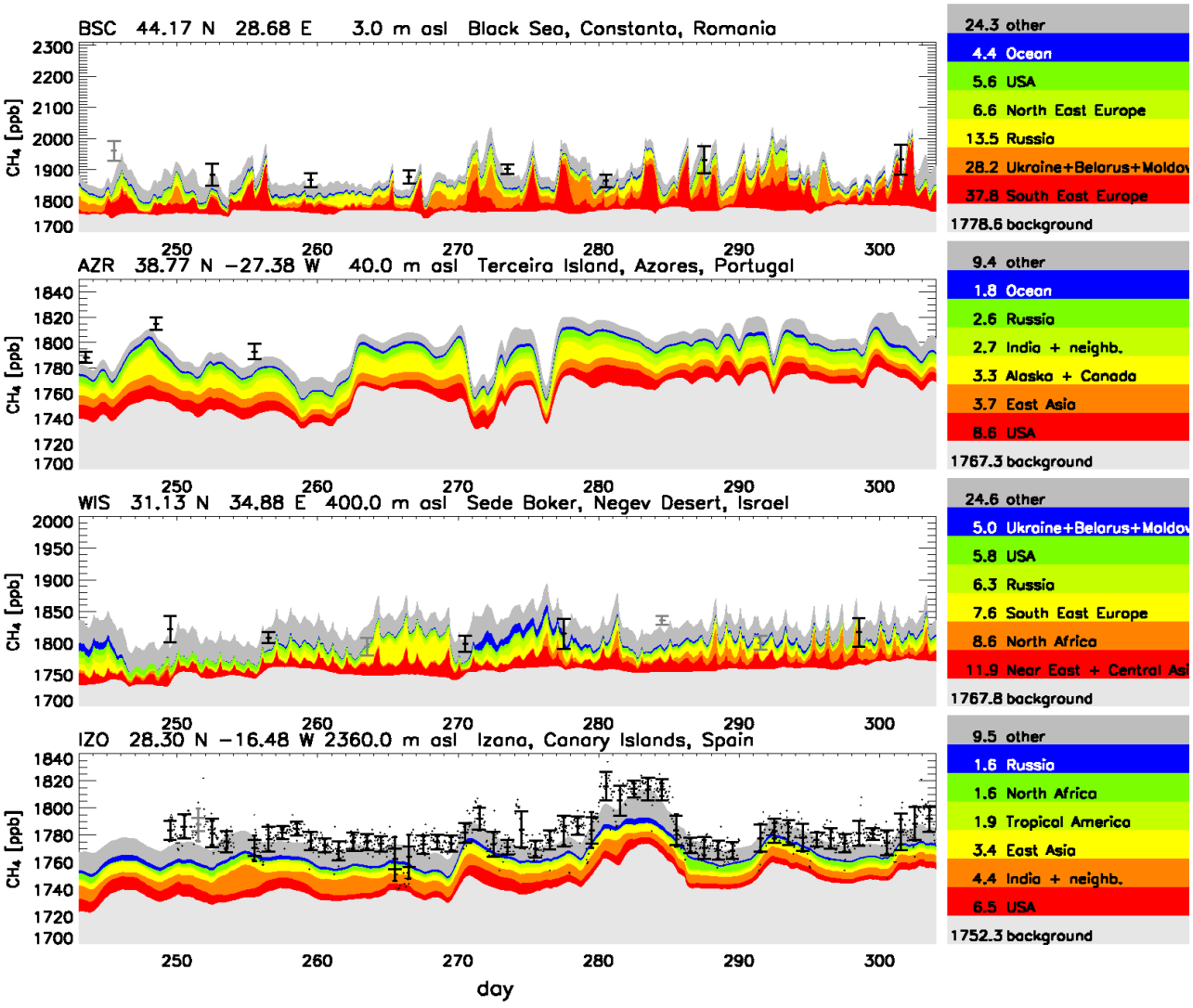

Fig. 6. Continued.

intervals of 1 sample/week. For sites with strong regional source contributions (e.g. HUN and BSC), the flask observations provide a fragmentary picture only. Nevertheless, also these observations are useful for further constraining the inversion (as will be shown in Sect. 3.2.2 and Table 6).

3.1.2 Global sites

A selected set of global sites is shown in Fig. 7 (for the complete set, see the figures available on our ftp server). In general, most global sites have a weaker total "direct source contribution" than the European continental sites, and hence more remote character. In the NH many global sites are in the range of ∼30–70 ppb. The total direct source contribution decreases further at the tropical sites (10–30 ppb) and in the extra-tropical SH. All sites south of 45° S exhibit a total direct source contribution of <10 ppb, and the minimum is reached at SPO (3.1 ppb). The figure illustrates the consistency of modelled CH_4 mixing ratios with measurements throughout the globe, including the high latitude SH background sites. Although this study does not primarily focus on the global inversion, consistent global CH_4 fields are important as significant long range transport is seen at all European sites.

Several remote marine sites are significantly influenced by variations of the background rather than direct source influence (in particular in the tropics (e.g. Mauna Loa (MLO), Cape Kumukahi (KUM), Ragged Point (RPB)), where the average NS gradient of CH_4 mixing ratios is large).

Illustrative is the comparison of the two "adjacent" sites, MLO and KUM. Separated by less than 100 km, but very different in their altitude (3397 m vs. 3 m a.s.l.), they show very different regional contributions. For example, the average

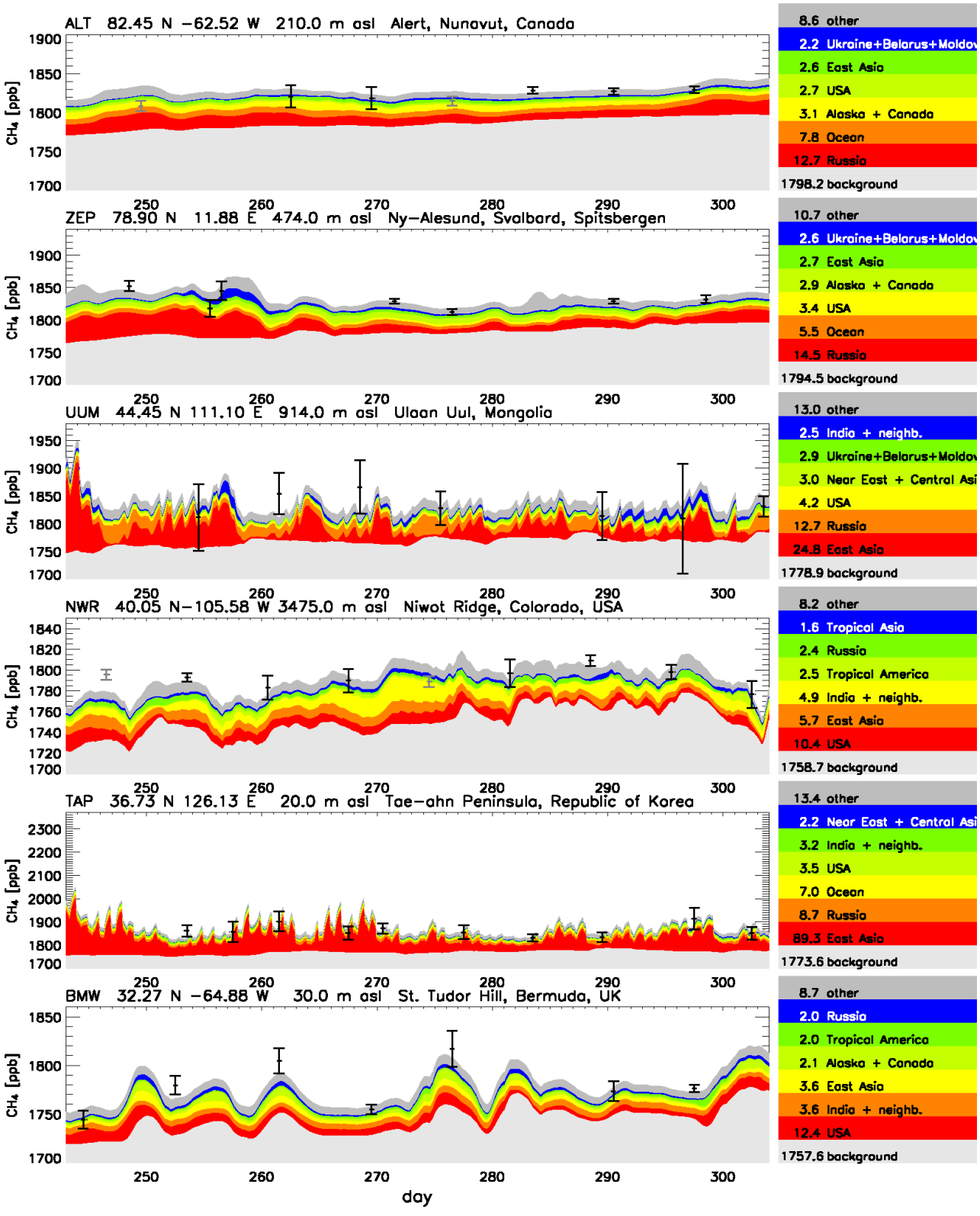

Fig. 7. Observed and modeled CH_4 at some global sites for September and October 2001.

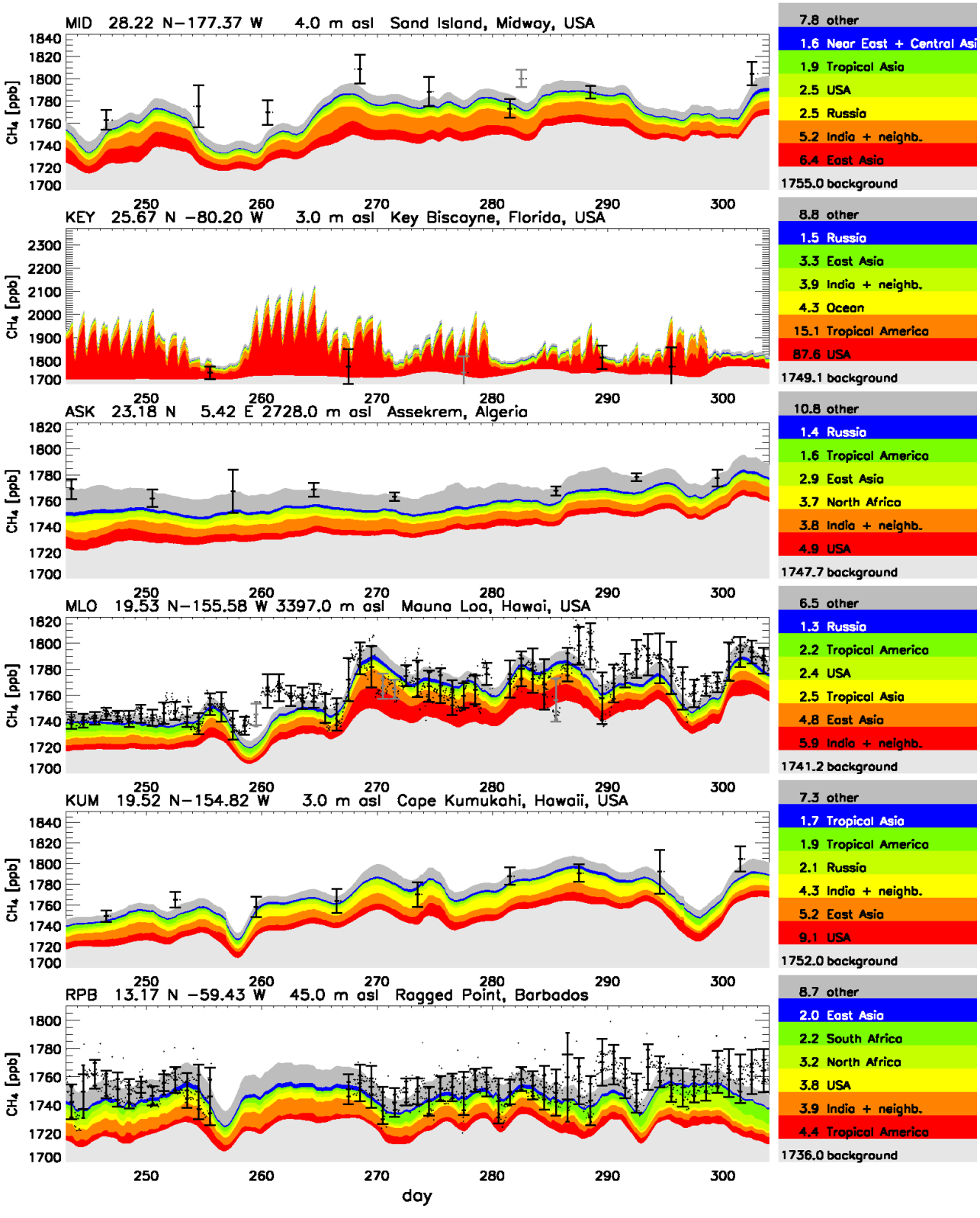

Fig. 7. Continued.

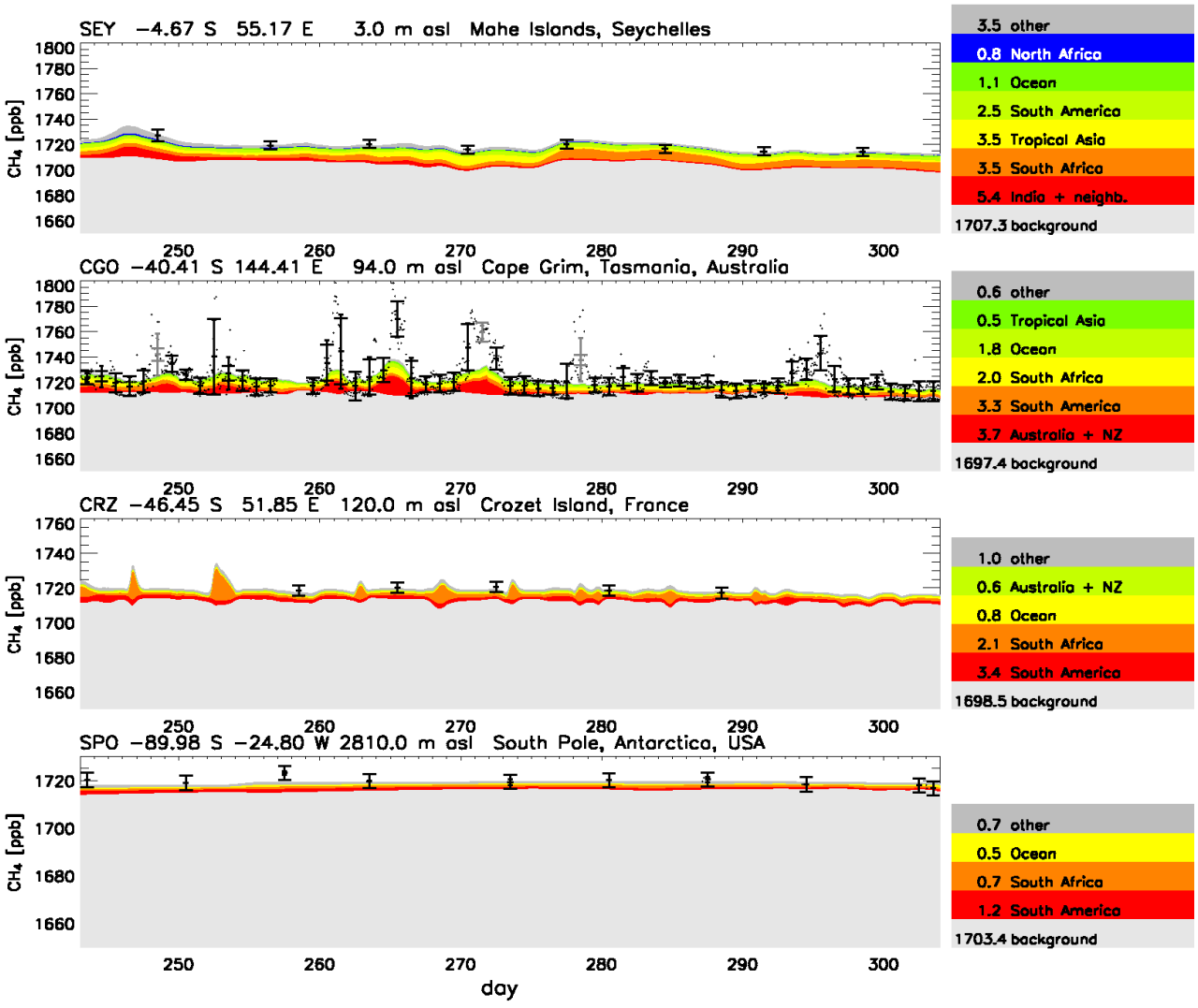

Fig. 7. Continued.

contribution from USA is 9.1 ppb at KUM, but only 2.4 ppb at MLO, although the total direct source contribution is comparable at both sites (MLO: 25.6 ppb, KUM 31.6 ppb).

At Cape Grim (CGO), events with significantly elevated CH_4 mixing rations are observed, which are usually not (or not well) reproduced by the model. Many of these events, however, are rejected by the iterative inversion procedure (according Eq. 11).

In general, the measurements at all European and most global sites are reproduced quite well, including the 3-D spatial gradient, the seasonal cycles and the short-term synoptic variability.

3.2 A posteriori inventories and sensitivity experiments

A posteriori emissions are compiled for various scenarios in Tables 4 and 5 and summarized in Table 1. The base scenario is denoted S1, while scenarios S2–S4 use slightly different sets of sites; in scenarios S5–S7 different weighting factors for the observations were applied, and in scenarios S8–S9 the influence of the OH sink is investigated. First we discuss some features which are apparent in all scenarios, while the influence of parameters which have been varied in the individual scenarios are discussed in the subsequent sections.

For the European regions, the strongest constraints are on emissions from Germany, France, BENELUX, UK, and Ireland due to the set of available observations, which is strongly biased towards Western European countries. Emissions from several of these countries are higher than a priori values, especially France, where the a posteriori emission increase is +73% (average of scenarios S1–S9), while smaller increases are derived for Germany (+7%), UK (+26%), and BENELUX (+9%). The a posteriori total for all EU-15 countries, however, is virtually identical to the a priori value,

Table 4. Overview of various inversion scenarios. Scenarios S1–S4 use different sets of sites. In scenarios S5–S7 the weighting factors $\alpha_{i\,\mathrm{FM}}$ and $\alpha_{i\,\mathrm{CM}}$ for the observations are varied, while in scenarios S8 and S9 the influence of the OH sink has been investigated (scaling of global OH field with β_{OH}). n_{data} denotes the dimension of the observational space (i.e. number of observations), and $n_{\mathrm{data\,eff}}$ is the "effective dimension", i.e. weighted with the $\alpha_{i\,\mathrm{FM}}$ and $\alpha_{i\,\mathrm{CM}}$ of the individual observations. Chi-square, defined as $\chi^2 = \frac{1}{n}\sum_{i=1}^{n}\frac{[\mathrm{CH_{4\,model},}_i - \mathrm{CH_{4\,obs},}_i]^2}{\Delta\mathrm{CH}^2_{4\,\mathrm{data},i}}$, is given for a priori and a posteriori (1st and 2nd iteration) model simulations.

sites	S1 all	S2 as S1 except DEU, SAC	S3 as S1 except ZGT, KOL, DEU, SAC	S4 as S1 but MHD−2° W and sel. obs.	S5 as S1	S6 as S1	S7 as S3	S8 as S1	S9 as S1
$\alpha_{i\,\mathrm{FM}}$	1/2	1/2	1/2	1/2	1/4	1/6	1/6	1/2	1/2
$\alpha_{i\,\mathrm{CM}}$	1/6	1/6	1/6	1/6	1/12	1/18	1/18	1/6	1/6
β_{OH}	1.00	1.00	1.00	1.00	1.00	1.00	1.00	0.95	1.05
n_{para}	496	496	496	496	496	496	496	496	496
n_{data}	6494	5992	5264	6396	6468	6455	5230	6501	6485
$n_{\mathrm{data\,eff}}$	1702.3	1619.3	1496	1684.3	845.5	561.7	493.9	1703.8	1700.5
χ^2 (a priori)	3.62	3.67	3.70	3.72	3.62	3.62	3.70	5.03	2.20
χ^2 (a posteriori, 1st iteration)	1.96	1.96	1.98	2.05	2.01	2.04	2.07	1.95	1.98
χ^2 (a posteriori, 2nd iteration)	0.76	0.77	0.77	0.77	0.78	0.79	0.80	0.76	0.77

Table 5. A posteriori emissions from scenarios S1–S9. Emissions are given in Tg CH_4/yr ($\pm 1\sigma$).

	a priori	S1	S2	S3	S4	S5	S6	S7	S8	S9
EU-15										
Germany	3.88±0.96	3.96±0.27	4.87±0.32	4.52±0.42	3.90±0.27	3.92±0.36	3.94±0.41	4.32±0.59	3.94±0.27	3.96±0.27
Italy	2.02±0.59	2.17±0.42	2.15±0.43	2.16±0.43	2.13±0.43	2.13±0.48	2.10±0.51	2.14±0.51	2.16±0.42	2.19±0.43
France	2.56±0.63	4.58±0.25	4.62±0.34	4.71±0.35	4.48±0.25	4.32±0.31	4.13±0.35	3.86±0.46	4.57±0.25	4.60±0.25
BENELUX	1.47±0.34	1.66±0.16	1.60±0.17	1.35±0.19	1.66±0.16	1.67±0.20	1.66±0.23	1.47±0.25	1.66±0.16	1.66±0.16
Austria	0.32±0.08	0.30±0.07	0.29±0.07	0.28±0.07	0.30±0.07	0.30±0.07	0.30±0.07	0.30±0.07	0.30±0.07	0.30±0.07
Spain	1.84±0.49	2.03±0.43	2.04±0.44	2.00±0.44	1.99±0.43	1.98±0.45	1.96±0.46	1.97±0.46	2.00±0.43	2.03±0.43
Portugal	0.37±0.11	0.39±0.11	0.39±0.11	0.38±0.11	0.38±0.11	0.38±0.11	0.38±0.11	0.38±0.11	0.39±0.11	0.39±0.11
UK	3.35±1.21	4.39±0.41	4.21±0.44	3.97±0.46	4.00±0.43	4.33±0.54	4.27±0.62	3.91±0.68	4.38±0.41	4.40±0.41
Ireland	0.64±0.17	0.26±0.06	0.27±0.06	0.28±0.06	0.75±0.15	0.31±0.08	0.34±0.09	0.35±0.09	0.26±0.06	0.26±0.06
Greece	0.40±0.11	0.39±0.11	0.39±0.11	0.39±0.11	0.39±0.11	0.40±0.11	0.40±0.11	0.40±0.11	0.39±0.11	0.39±0.11
Sweden	1.08±0.46	0.91±0.37	0.89±0.38	0.97±0.38	0.86±0.37	0.92±0.40	0.97±0.42	0.99±0.42	0.89±0.37	0.92±0.37
Finland	3.23±1.40	−0.10±0.80	−0.27±0.79	−0.21±0.81	−0.12±0.80	0.68±0.95	1.26±1.04	1.30±1.05	0.00±0.80	−0.14±0.80
Denmark	0.34±0.09	0.34±0.07	0.33±0.07	0.30±0.08	0.34±0.07	0.34±0.08	0.33±0.08	0.32±0.09	0.34±0.07	0.34±0.07
Total EU-15	21.51±2.40	21.28±1.02	21.77±1.04	21.11±1.07	21.05±1.02	21.69±1.24	22.03±1.37	21.71±1.45	21.28±1.02	21.31±1.02
Other European										
Switzerland	0.17±0.05	0.19±0.05	0.19±0.05	0.20±0.05	0.20±0.05	0.19±0.05	0.18±0.05	0.19±0.05	0.19±0.05	0.20±0.05
Norway	0.22±0.07	0.22±0.07	0.22±0.07	0.22±0.07	0.22±0.07	0.22±0.07	0.22±0.07	0.22±0.07	0.22±0.07	0.22±0.07
North East Europe	5.76±1.49	4.15±0.56	4.02±0.57	4.24±0.63	4.16±0.56	4.44±0.71	4.57±0.81	4.63±0.87	4.17±0.56	4.17±0.56
South East Europe	6.75±1.78	4.65±0.77	4.59±0.77	4.56±0.77	4.79±0.75	4.91±0.95	5.04±1.07	4.99±1.07	4.83±0.75	4.60±0.77
Global regions										
Ukraine + Belarus + Moldova	10.23±2.59	8.77±1.25	8.72±1.26	9.00±1.28	8.75±1.25	8.60±1.50	8.63±1.64	8.78±1.66	8.69±1.25	8.79±1.25
Alaska + Canada	9.35±4.13	11.26±0.94	10.71±0.96	10.62±0.96	11.69±0.92	10.61±1.25	10.45±1.48	9.94±1.48	11.11±0.94	11.41±0.94
USA	28.28±6.25	35.59±1.82	35.04±1.82	35.14±1.82	36.76±1.82	36.20±2.41	36.20±2.82	35.85±2.82	35.01±1.82	36.39±1.82
Tropical America	20.41±4.67	25.76±3.23	25.67±3.23	25.61±3.23	25.41±3.23	24.02±3.68	23.30±3.90	23.33±3.90	24.26±3.22	27.64±3.23
South America	59.16±14.69	48.12±5.23	48.07±5.23	48.05±5.23	48.20±5.23	50.28±6.14	50.98±6.69	50.91±6.69	42.72±5.23	53.86±5.22
North Africa	42.35±10.16	18.57±3.27	18.72±3.27	18.83±3.27	17.78±3.26	24.82±4.23	27.35±4.76	27.70±4.77	15.08±3.21	20.81±3.27
South Africa	36.96±9.30	50.25±4.66	50.24±4.66	50.19±4.66	50.48±4.66	46.53±5.41	44.98±5.83	45.00±5.83	48.42±4.66	52.28±4.66
Near East + Central Asia	21.15±6.58	19.07±2.39	18.89±2.40	18.68±2.40	19.24±2.40	18.24±3.12	18.31±3.57	18.28±3.57	18.66±2.39	18.97±2.40
Russia	43.89±15.07	29.30±2.09	29.96±2.09	29.96±2.11	28.59±2.07	28.25±2.70	27.14±3.13	27.68±3.13	28.29±2.08	29.99±2.09
East Asia	59.87±13.78	43.96±3.19	44.00±3.19	44.15±3.19	43.89±3.19	46.61±4.25	48.51±5.00	48.73±5.01	43.30±3.19	44.80±3.19
India + neighb.	64.48±14.63	84.11±6.33	84.38±6.33	84.70±6.33	83.58±6.33	78.00±7.69	75.21±8.45	75.30±8.44	80.50±6.33	88.33±6.34
Tropical Asia	60.50±16.24	61.43±6.70	61.52±6.70	61.49±6.70	61.83±6.70	62.13±7.98	62.24±8.75	62.09±8.75	54.79±6.70	68.22±6.70
Australia + NZ	14.84±4.33	9.76±2.66	9.75±2.66	9.74±2.66	9.74±2.66	10.29±3.09	10.84±3.33	10.85±3.33	9.24±2.63	10.09±2.65
Greenland	0.20±0.10	0.13±0.07	0.13±0.07	0.14±0.07	0.15±0.07	0.15±0.08	0.19±0.09	0.19±0.08	0.13±0.07	0.13±0.07
Total	525.65±38.19	496.09±3.76	496.10±3.76	496.14±3.76	496.01±3.76	495.71±4.79	495.93±5.49	495.92±5.49	470.41±3.76	521.72±3.77

but with substantially reduced uncertainty (from 2.4 to 1.0–1.4 Tg CH_4/yr). The a posteriori increase of the abovementioned countries is mainly balanced by a strong decrease of CH_4 emissions from Finland, for which in scenarios S1–S4 values close to zero are derived (nominally even negative values, but these are not significantly different from zero or the pure anthropogenic part of the CH_4 emissions (0.24 Tg CH_4/yr as derived from the bottom-up inventory; Table 1)). This result suggests that emissions from the wetlands in Finland are much smaller than predicted by the a priori inventory (3.0 Tg CH_4/yr).

As the direct signal from Finland at the observational sites available in this study is relatively weak (and flask sampling at Pallas started only at the end of 2001), this result has to be interpreted with some caution. In order to further investigate the impact of Finnish emissions we have performed forward simulations for year 2002 and compared them with observations at Pallas (Fig. 9). This exercise clearly demonstrates that the emissions based on the Walter et al. (2001a) inventory lead to much higher CH_4 mixing ratios in summer than observed. In contrast, forward simulations based on the a posteriori inventory of year 2001 (from scenario S1) yield CH_4 mixing ratios very close to observations for year 2002. An additional model simulation, based on the a priori inventory for year 2001, but with emissions of the Pallas $3^\circ \times 2^\circ$ grid cell switched off, shows that the influence of local emissions is relatively small, i.e. that the discrepancy between simulations and observations mainly arises from the large scale influence of the Finnish wetlands (from the Walter et al. (2001a) inventory).

Furthermore, all inversion scenarios indicate somewhat smaller emissions for Sweden, which is also strongly influenced by natural wetlands.

On the global scale the most prominent features, compared to a priori values, are smaller emissions for North Africa, Russia, East Asia, and higher emissions for USA, South Africa, and India+neighbouring countries.

All scenarios lead to significant reductions of χ^2 from a priori values of 3.62–3.72 to 1.96–2.07 in the first iteration, and 0.76–0.80 in the second iteration (Table 4). This strong final reduction of χ^2 is mainly due to the rejection of outliers (while a posteriori emissions derived in both iterations usually do not differ very much).

3.2.1 Influence of different sets of sites

Compared to the base scenario S1, we omitted some European sites with very strong regional influence in scenarios S2 (without Deusselbach (DEU) and Saclay (SAC)) and S3 (without Zingst (ZGT), Kollumerwaard (KOL), DEU, and SAC) (see also Table 3). The most evident effect is an increase in German emissions, as, in particular, inclusion of DEU results in significantly smaller a posteriori German emissions (see Sect. 3.2.2, and Table 6). As already mentioned, however, this leads to a redistribution of calculated emissions among the European countries, while the EU-15 total remains virtually unchanged.

A particularly critical site appears to be Mace Head (MHD), as the corresponding $1^\circ \times 1^\circ$ grid largely covers land masses with significant CH_4 emissions. Although the a posteriori CH_4 mixing ratios agree quite favourably with the observations, situations with westerly winds from the Atlantic may be biased (with model results affected by Irish emissions, but not the observations). Thus the very low CH_4 emissions derived for Ireland in scenarios S1–S3 are to some extent due to this effect. The ^{222}Rn experiments showed that much better agreement with observations can be achieved if the model is sampled at a virtual site, shifted by 2° to the west. Tentatively we also applied this shift to the CH_4 inversion while excluding observations with strong regional influence (denoted by "P" flag in the AGAGE data set), because the shifted model site is unlikely to reproduce regional pollution events correctly. The corresponding inversion scenario S4 shows – compared to S1–S3 – much higher CH_4 emissions for Ireland that are close to the a priori value. It is difficult to judge which type of sampling is more appropriate, since both approaches clearly imply some systematic biases which are difficult to quantify. Consequently, the exact attribution of the Mace Head observations to emissions in Ireland should be interpreted with care.

3.2.2 Influence of individual European sites

In order to further investigate the impact of individual sites we performed inversions using single European sites only. The results are compiled in Table 6 and further illustrate the different character of the different sites. Sites which are strongly influenced by regional emissions like Zingst (ZGT), Neuglobsow (NGB) and Deusselbach (DEU) lead to distinct reductions of calculated a posteriori uncertainties and frequently to significant shifts of the a posteriori fluxes. Clearly, the impact of these sites has to be viewed quite critically since their influence on derived emissions from a whole region might be too strong. This so-called aggregation error has been observed in global inversions, when big regions are used (Kaminski et al., 2001).

Saclay (SAC), despite its semi-urban character and proximity to Paris, has only a moderate impact on French a posteriori emissions (increase of emissions by 14%, reduction of uncertainty by 26%). Most other single sites, however, also lead to a small increase of computed emissions from France. Obviously, this effect is augmented in the inversion with the (more or less) complete set of sites in scenarios S1–S4.

Also, all single sites indicate reduced emissions from Finland, typically in the order of 1–20%. This effect is enhanced in the full inversion (scenarios S1–S9) leading to net emissions from Finland close to zero.

Further investigation of the base functions from Finland show the very strong signals during summer. E.g. for emissions of July and August at the sites Zingst (ZGT) or Baltic

Table 6. European a posteriori emissions using single European sites only (units are in Tg CH_4/yr). Large shifts in emissions and significant uncertainty reductions are highlighted by the colors (see legend below).

	a priori	ZGT	KOL	MHD	MHD -2W / sel. obs.	NGB	CB4
Germany	3.88 ± 0.96	4.63 ± 0.51	3.47 ± 0.69	3.76 ± 0.93	3.61 ± 0.94	2.10 ± 0.35	3.31 ± 0.76
Italy	2.02 ± 0.59	2.02 ± 0.59	2.01 ± 0.59	2.01 ± 0.59	1.98 ± 0.59	2.10 ± 0.59	2.00 ± 0.59
France	2.56 ± 0.63	2.70 ± 0.62	2.71 ± 0.63	2.78 ± 0.61	2.49 ± 0.63	2.76 ± 0.61	2.72 ± 0.60
BENELUX	1.47 ± 0.34	1.67 ± 0.32	1.61 ± 0.28	1.44 ± 0.34	1.43 ± 0.34	1.56 ± 0.32	1.31 ± 0.26
Austria	0.32 ± 0.08	0.32 ± 0.08	0.32 ± 0.08	0.32 ± 0.08	0.32 ± 0.08	0.33 ± 0.08	0.32 ± 0.08
Spain	1.84 ± 0.49	1.88 ± 0.48	1.86 ± 0.49	1.88 ± 0.48	1.81 ± 0.48	1.86 ± 0.48	1.85 ± 0.48
Portugal	0.37 ± 0.11	0.38 ± 0.11	0.38 ± 0.11	0.37 ± 0.11	0.37 ± 0.11	0.38 ± 0.11	0.38 ± 0.11
UK	3.35 ± 1.21	3.96 ± 0.98	3.58 ± 1.11	3.96 ± 0.88	2.68 ± 0.95	3.72 ± 1.04	3.06 ± 0.87
Ireland	0.64 ± 0.17	0.65 ± 0.17	0.65 ± 0.17	0.39 ± 0.08	0.70 ± 0.16	0.64 ± 0.17	0.64 ± 0.17
Greece	0.40 ± 0.11	0.40 ± 0.11	0.40 ± 0.11	0.40 ± 0.11	0.40 ± 0.11	0.40 ± 0.11	0.40 ± 0.11
Sweden	1.08 ± 0.46	1.01 ± 0.46	1.07 ± 0.46	1.04 ± 0.46	1.05 ± 0.46	1.03 ± 0.46	1.04 ± 0.46
Finland	3.23 ± 1.40	2.73 ± 1.30	3.14 ± 1.40	3.02 ± 1.39	3.06 ± 1.37	2.70 ± 1.37	3.05 ± 1.39
Denmark	0.34 ± 0.09	0.27 ± 0.08	0.33 ± 0.09	0.34 ± 0.09	0.33 ± 0.09	0.32 ± 0.09	0.33 ± 0.09
Switzerland	0.17 ± 0.05	0.17 ± 0.05	0.17 ± 0.05	0.17 ± 0.05	0.17 ± 0.05	0.17 ± 0.05	0.17 ± 0.05
Norway	0.22 ± 0.07	0.22 ± 0.07	0.22 ± 0.07	0.22 ± 0.07	0.22 ± 0.07	0.22 ± 0.07	0.22 ± 0.07
North East Europe	5.76 ± 1.49	4.33 ± 0.98	5.57 ± 1.45	5.65 ± 1.46	5.37 ± 1.45	4.29 ± 0.94	5.58 ± 1.45
South East Europe	6.75 ± 1.78	6.40 ± 1.74	6.57 ± 1.78	6.56 ± 1.78	6.49 ± 1.78	6.66 ± 1.76	6.56 ± 1.78

	a priori	DEU	SAC	SIL	SIL selected obs	ZUG	ZUG selected obs
Germany	3.88 ± 0.96	2.26 ± 0.49	4.26 ± 0.88	3.89 ± 0.63	3.63 ± 0.60	4.40 ± 0.85	4.38 ± 0.83
Italy	2.02 ± 0.59	1.97 ± 0.59	2.03 ± 0.59	1.81 ± 0.53	1.81 ± 0.51	2.00 ± 0.54	1.93 ± 0.52
France	2.56 ± 0.63	3.05 ± 0.50	2.92 ± 0.47	2.68 ± 0.53	2.81 ± 0.51	2.52 ± 0.61	2.50 ± 0.60
BENELUX	1.47 ± 0.34	1.41 ± 0.30	1.60 ± 0.32	1.56 ± 0.32	1.52 ± 0.32	1.48 ± 0.34	1.50 ± 0.33
Austria	0.32 ± 0.08	0.32 ± 0.08	0.32 ± 0.08	0.32 ± 0.08	0.32 ± 0.08	0.32 ± 0.08	0.32 ± 0.08
Spain	1.84 ± 0.49	1.84 ± 0.48	1.80 ± 0.48	1.76 ± 0.47	1.73 ± 0.46	1.82 ± 0.48	1.84 ± 0.47
Portugal	0.37 ± 0.11	0.37 ± 0.11	0.37 ± 0.11	0.37 ± 0.11	0.37 ± 0.11	0.38 ± 0.11	0.38 ± 0.11
UK	3.35 ± 1.21	3.52 ± 0.95	3.67 ± 1.05	3.94 ± 0.87	3.80 ± 0.86	3.35 ± 1.10	3.66 ± 1.07
Ireland	0.64 ± 0.17	0.65 ± 0.17	0.65 ± 0.17	0.66 ± 0.17	0.66 ± 0.17	0.64 ± 0.17	0.65 ± 0.17
Greece	0.40 ± 0.11	0.40 ± 0.11	0.40 ± 0.11	0.40 ± 0.11	0.40 ± 0.11	0.40 ± 0.11	0.40 ± 0.11
Sweden	1.08 ± 0.46	1.02 ± 0.46	1.06 ± 0.46	0.99 ± 0.45	0.99 ± 0.45	1.05 ± 0.46	1.06 ± 0.46
Finland	3.23 ± 1.40	2.90 ± 1.38	3.15 ± 1.39	2.85 ± 1.38	2.75 ± 1.37	3.05 ± 1.39	3.11 ± 1.39
Denmark	0.34 ± 0.09	0.33 ± 0.09	0.34 ± 0.09	0.34 ± 0.09	0.33 ± 0.09	0.34 ± 0.09	0.34 ± 0.09
Switzerland	0.17 ± 0.05	0.16 ± 0.05	0.17 ± 0.05	0.17 ± 0.05	0.17 ± 0.05	0.17 ± 0.05	0.17 ± 0.05
Norway	0.22 ± 0.07	0.22 ± 0.07	0.22 ± 0.07	0.22 ± 0.07	0.22 ± 0.07	0.22 ± 0.07	0.22 ± 0.07
North East Europe	5.76 ± 1.49	4.92 ± 1.36	5.74 ± 1.48	5.58 ± 1.38	5.64 ± 1.35	5.58 ± 1.34	5.65 ± 1.35
South East Europe	6.75 ± 1.78	6.59 ± 1.78	6.71 ± 1.78	6.64 ± 1.77	6.63 ± 1.77	6.62 ± 1.76	6.63 ± 1.76

	a priori	IZO	BAL	HUN	BSC
Germany	3.88 ± 0.96	3.87 ± 0.95	4.34 ± 0.74	3.56 ± 0.87	3.87 ± 0.95
Italy	2.02 ± 0.59	2.02 ± 0.59	2.07 ± 0.59	2.03 ± 0.57	2.05 ± 0.59
France	2.56 ± 0.63	2.55 ± 0.63	2.69 ± 0.62	2.63 ± 0.63	2.58 ± 0.63
BENELUX	1.47 ± 0.34	1.47 ± 0.34	1.56 ± 0.33	1.50 ± 0.33	1.47 ± 0.34
Austria	0.32 ± 0.08	0.32 ± 0.08	0.32 ± 0.08	0.28 ± 0.08	0.32 ± 0.08
Spain	1.84 ± 0.49	1.82 ± 0.48	1.85 ± 0.49	1.90 ± 0.48	1.85 ± 0.49
Portugal	0.37 ± 0.11	0.37 ± 0.11	0.38 ± 0.11	0.38 ± 0.11	0.38 ± 0.11
UK	3.35 ± 1.21	3.36 ± 1.21	2.99 ± 0.95	3.57 ± 1.19	3.40 ± 1.21
Ireland	0.64 ± 0.17	0.64 ± 0.17	0.62 ± 0.17	0.65 ± 0.17	0.64 ± 0.17
Greece	0.40 ± 0.11	0.40 ± 0.11	0.40 ± 0.11	0.40 ± 0.11	0.40 ± 0.11
Sweden	1.08 ± 0.46	1.07 ± 0.46	0.93 ± 0.43	1.06 ± 0.46	1.08 ± 0.46
Finland	3.23 ± 1.40	3.20 ± 1.40	2.61 ± 1.25	3.08 ± 1.39	3.08 ± 1.38
Denmark	0.34 ± 0.09	0.34 ± 0.09	0.28 ± 0.09	0.33 ± 0.09	0.34 ± 0.09
Switzerland	0.17 ± 0.05	0.17 ± 0.05	0.17 ± 0.05	0.17 ± 0.05	0.17 ± 0.05
Norway	0.22 ± 0.07	0.22 ± 0.07	0.22 ± 0.07	0.22 ± 0.07	0.22 ± 0.07
North East Europe	5.76 ± 1.49	5.75 ± 1.48	4.96 ± 1.02	3.70 ± 0.94	5.42 ± 1.38
South East Europe	6.75 ± 1.78	6.71 ± 1.78	6.74 ± 1.75	5.68 ± 1.37	5.57 ± 1.26

a posteriori emission
>1.3
1.2-1.3
1.1-1.2
0.9-1.1
0.8-0.9
0.7-0.8
<0.7

a posteriori uncertainty
<0.4
0.6-0.4
0.8-0.6
1.0-0.8

sea (BAL) (which are the stations closest to the Finnish wetlands) signals of up to 40–60 ppb for single days (daily average) are simulated. Even at Schauinsland (SIL) daily average signals of up to 3.7 ppb are calculated. Obviously these strong signals are not consistent with the observations, leading the inversion to drastically reduce the contribution from the Finnish summer base functions (for comparison, the influence of winter base functions from Finland is typically below 1 ppb at BAL and ZGT).

For most other countries, however, the analysis from the single site inversion is more ambiguous; e.g. for Germany or BENELUX, both increased and decreased emissions were found (reflected in the full inversion by only small shifts of a posteriori emissions).

It is interesting to note that the flask sampling sites in Eastern Europe (Baltic Sea (BAL), Hegyatsal (HUN)) put significant constraints on emissions from Germany and the UK.

We also used the single site experiments to further check the impact of data selection procedures applied at a few sites (see Sect. 2.4).

For Schauinsland (SIL) the use of night-time data only indeed leads to slightly smaller derived CH_4 emissions from Germany. In the non-selected case the observed upslope winds during summer daytime (which are not reproduced in the model) need to be compensated in the inversion by artificially higher German emission. This effect, however, is relatively small ($\sim$7% difference of deduced German emissions), and even much smaller for Zugspitze (ZUG) (difference $\sim$0.5%).

As already observed in the full inversion, the effect of shifting the site Mace Head (MHD) and selecting "non-polluted" data only, is considerable (difference of derived Irish emission of 78% (0.31 Tg CH_4/yr)).

3.2.3 Influence of weighting factor for observations

As described in Sect. 2.3, a weighting factor is applied to reduce the strong bias of the inversion towards observation space. Using the default values of $\alpha_{i\,\mathrm{FM}}$=1/2 for flask samples and $\alpha_{i\,\mathrm{CM}}$=1/6 for daily averages of continuous measurements, the inversion is still dominated by the observations ("effective" dimension of observational space in scenario S1: 1702 (see Table 4) vs. dimension of parameter space (n_{para}): 496). In scenarios S5 and S6 we further decrease the weighting of observations to $\alpha_{i\,\mathrm{FM}}$=1/4, $\alpha_{i\,\mathrm{CM}}$=1/12 (S5) and $\alpha_{i\,\mathrm{FM}}$=1/6, $\alpha_{i\,\mathrm{CM}}$=1/18 (S5), bringing the effective dimension of the observational space closer to the dimension of the parameter space. As expected, this leads to smaller reductions of calculated a posteriori uncertainties and, in general, to smaller shifts of a posteriori emissions compared to a priori values. It is interesting to note, however, that the latter not always increase or decrease monotonously towards the a priori values with decreasing weighting factor. This is obviously due to the very complex structure of the cost function. With decreasing weight of observations, the a posteriori emissions from Finland increase slightly (compared to values close to zero in scenarios S1–S4). Even in scenario S6, however, the emissions from Finland are only 39% of the a priori estimate, which is a clear indication that the bottom-up estimate (which was dominated by estimated 3 Tg CH_4/yr from wetlands) for Finland is likely too high (see also Sects. 3.2, 3.2.2., and 3.3.2.).

Evidently the best choice of the weighting factors for the observations is not precisely defined and choosing them introduces a subjective component. We also tested the effect of including correlations in the data covariance matrix for observations of subsequent days. However, this leads to very small changes of a posteriori results only (results not shown). In numerical weather forecasting it has been observed that the use of positive observation error correlations reduces the weight given to the observations, and at the same time gives more relative importance to differences between observed values (Bouttier and Courtier, 1999). In our analysis, these two effects are balancing each other to some extent.

A final scenario, S7, uses the low weighting factors for observations and the reduced set of sites from scenario S3. Scenario S7, which can be considered as the most conservative scenario (putting relatively small weight on the observations, and omitting sites with large regional contributions), confirms the major principal features discussed for the other scenarios.

The lower weighting of observations leads to very small increases of χ^2 only, i.e. the fit to observations deteriorates only slightly (Table 4).

3.2.4 Influence of OH sink

In order to investigate the potential influence of the global OH sink we have generated an additional base function, in which the OH sink is simulated as negative CH_4 source (similar to the approach used by Hein et al. (1997), and Houweling et al. (1999)). Note that in the regular source functions used in our study the OH sink is already included. The new additional OH sink base function is added to these regular base functions (as additional term in Eq. 1). In this way we investigate the influence of -5% (scenario S8) and +5% (scenario S9) deviations in the global OH field (assuming, however, exactly the same spatio-temporal OH distribution). The resulting inversions show only a negligible influence on the results for the European countries. The change of approximately $-$/+5% in the total global CH_4 source strength (which is required in order to balance the $-$/+5% difference in the sink), is achieved mainly by those global regions, which cover the tropical areas (where the OH sink is largest). The results for the European countries show a remarkable stability with a maximum deviation between scenario S8 and S9 of 0.14 Tg CH_4/yr for Finland, even smaller deviations for the other European countries and a deviation of 0.03 Tg CH_4/yr for the EU-15 total (Table 5). This demonstrates that the emissions derived for European countries are

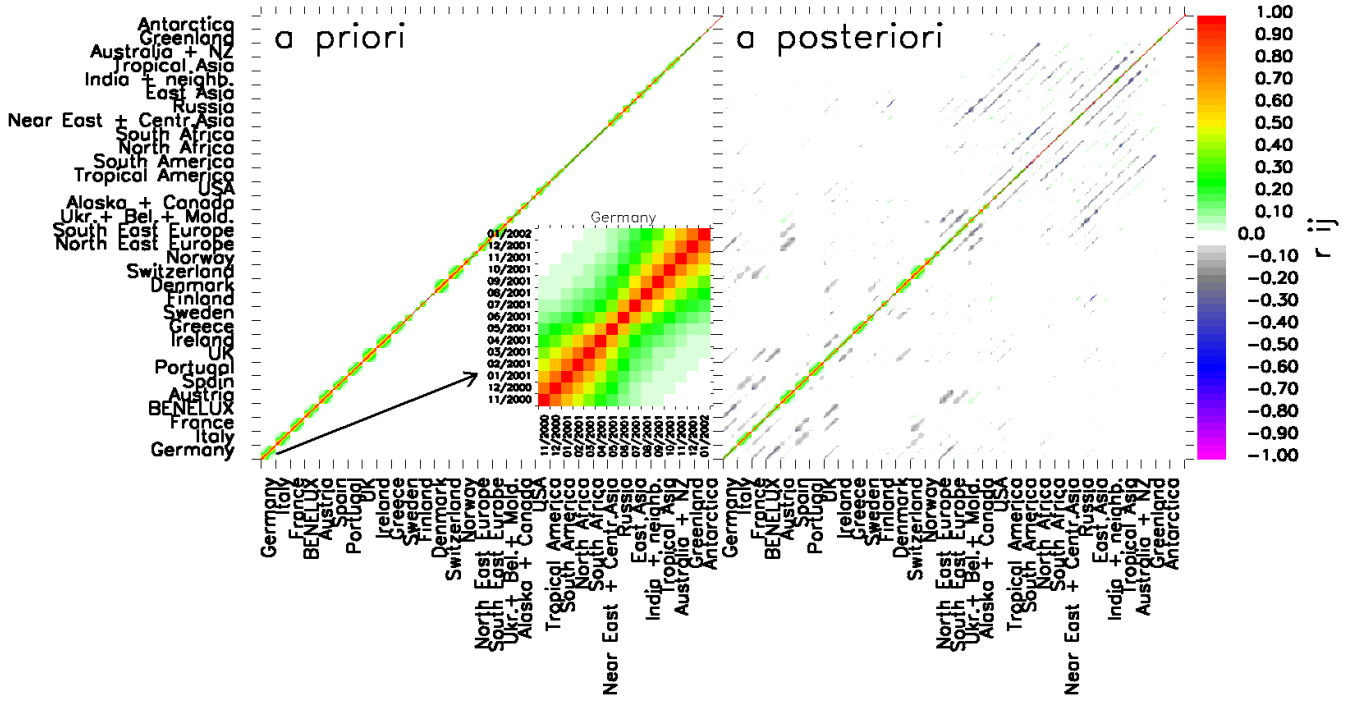

Fig. 8. Parameter covariance matrices. Left: a priori; right: a posteriori. For each region the emission of 2+12+1=15 months is shown (as illustrated in the zoomed view for a priori emissions from Germany).

strongly determined by the signals related to synoptic variations (which carry information from recent emissions which have not been influenced significantly by the OH sink).

3.2.5 A posteriori correlation of emissions

While the a priori emissions of different regions are assumed to be uncorrelated, the a posteriori emissions exhibit clear anti-correlations between different regions (Fig. 8). For example, the a posteriori emissions from Germany are significantly anti-correlated with the emissions from France, BENELUX, UK, and North East Europe. The figure shows that the anti-correlations in general extend over a relatively short temporal period (typically ±1–2 months); e.g. the emissions from Germany of one particular month are anticorrelated with the emission from the mentioned countries in the same months, or the preceding or following 1–2 months. Further prominent features are the anti-correlations of Ireland with UK and of Spain with Italy and France. This behavior is consistent with the abovementioned observation that, despite some differences for emissions from individual European countries in scenarios S1–S9, the EU-15 total emissions are relatively constant in all scenarios.

Furthermore, there are strong anti-correlations among the non-European global regions, For example, of tropical Asia with "India+neighboring countries" or of South Africa with South America and North Africa. In general, however, there are only weak anti-correlations between European and global regions, except for regions in the transition region from middle-west Europe to East Europe and Russia (including a weak anti-correlation between Finland and Russia). Also there are some weak anti-correlations between emissions from North America (USA, and Alaska+Canada) and some European countries.

3.2.6 Potential systematic errors

In the following we discuss the most important potential systematic errors which could affect the results of our study:

(1) In general, the Green's function approach is based on predefined relatively large regions, and may suffer from the aggregation error (Kaminski et al., 2001). The Green's function approach allows us to increase or decrease only the total emissions of the individual regions, but not to change the spatial emission distribution within the regions. The aggregation error is potentially most serious when including observations of strongly regional character (potentially leading to a shift in emissions of a whole larger region, although the influence area of these measurements might be much smaller). In fact scenarios S1–S4 show slightly different results (in particular for Germany and Ireland), however EU-15 total emissions are not affected significantly. Inverse approaches based on an adjoint model (Houweling et al., 1999; Kaminski et al., 1999a, b) or full 4DVAR data assimilation systems (Bouttier and Courtier, 1999; Engelen, 2004; Meirink et al., 2004) will allow a much higher degree of freedom in the parameter

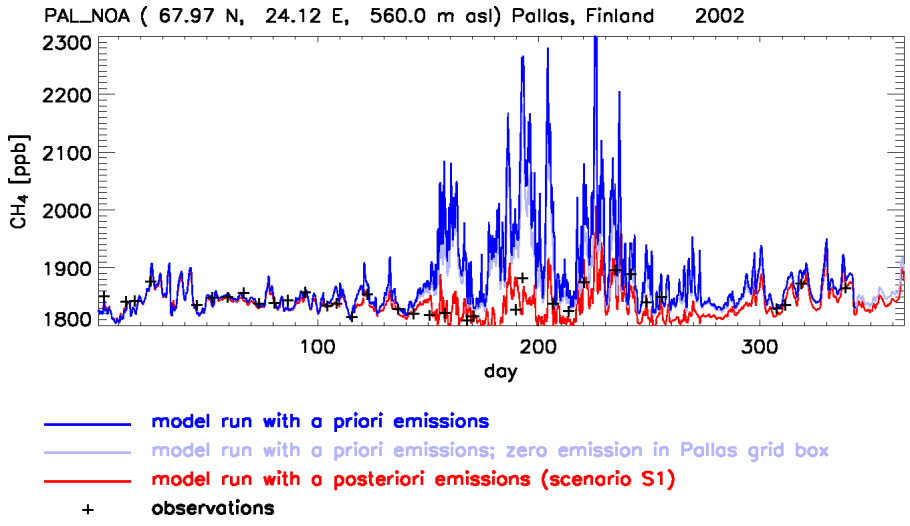

Fig. 9. Forward simulation for Pallas (PAL), Finland (year 2002) using the bottom-up inventory compiled in Table 1 (dark blue), and the a posteriori emissions from scenario S1 (red). Furthermore, simulations using the bottom-up inventory, but with emissions of the Pallas model grid cell switched off, are shown (light blue).

space (i.e. optimization of emissions from individual model grid cells), but will require, in practice, further assumptions about spatial correlations between emissions of different grid cells (making the inverse system stiffer, and probably similar to Green's function systems with relatively small regions).

(2) The representativeness error describes discrepancies in the behavior of a model grid cell (or interpolated point within that grid cell) with the real observational point, e.g. due to local meteorology which is not resolved in the model or strong emission gradients within a grid cell, as is frequently found at the land-sea border (such as for coastal sites like MHD). We addressed this potential error by data selection procedures for some sites (SIL and ZUG) and the general use of the 3-D model gradient as proxy for the representativeness error (Eq. 9). For MHD, in particular, the analysis remained ambiguous. Unfortunately, for many sites only limited information is available for further analysis (such as meteorology and measurements of other tracers, including ^{222}Rn).

(3) Systematic errors in model transport have a direct impact on the inversion results, and the inversion tends to compensate for these errors by erroneous adaptation of emissions. The TM5 model was intensively validated and compared with other models within the EVERGREEN projects, and the main transport features (such as vertical mixing or interhemispheric transport) are well within the range of other standard models. However, the TM5 model may have some tendency to underestimate vertical exchange, and it has recently been observed that enhancing the vertical mixing within the model boundary layer may further improve agreement with SF_6 observations (Peters et al., 2004). Since most CH_4 monitoring sites in Europe are in the boundary layer, however, enhanced vertical mixing in the model would most likely imply somewhat higher European CH_4 emissions resulting from the inversion.

(4) Some biases may be introduced by gaps in the observational records. In this study we did not apply further screening of observations but note that for several sites gaps exist within the analysis period, which may have some impact on the derived seasonal cycles of emissions. The requirement of contiguous observations, however, will be in particular important for multi year trend analyses (Rödenbeck et al., 2003).

(5) Furthermore, very different temporal resolution (monthly emissions vs. daily mean values of observations) and spatial scales (global vs. European zoom) may introduce some biases. While we tried to compensate for the different temporal scales by introducing the weighting factors α_i (equation (10)), no attempts have been made to correct for the different spatial scales. E.g. the assumption of a constant relative uncertainty per source category and region, independent of the size of the region and neglect of correlations between regions is equivalent to assuming a lower overall a priori uncertainty for the European total. In order to investigate a potential effect of the relatively small European/national regions on the estimate for the EU-15 total we performed an additional inversion, where the uncertainties of all European base functions were doubled (except Finland, where we kept the original uncertainty in order to avoid negative a posteriori emissions), but otherwise identical to scenario S1. The resulting a posteriori EU-15 total is 21.39±1.19 Tg CH_4/yr, i.e. very close to the value for scenario S1 (21.28±1.02 Tg CH_4/yr). This demonstrates that even relaxing the a priori uncertainties for the European countries, the EU-15 total estimates remain very stable.

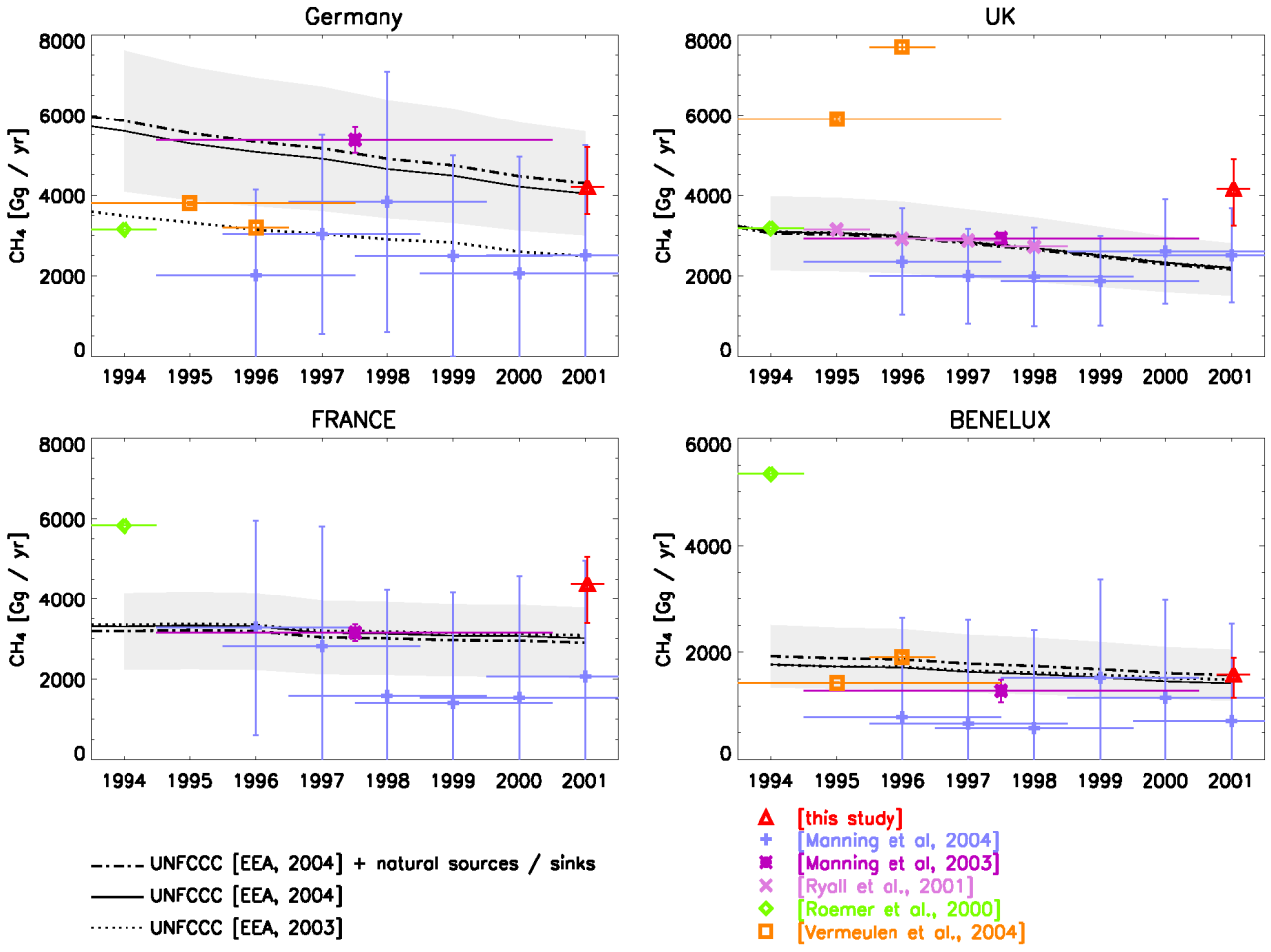

Fig. 10. Comparison with other inverse modelling studies and UNFCCC values. UNFCCC estimates (black solid curve) are augmented by our bottom-up estimate of net natural sources (including soil sink), displayed by the black dash-dotted line. The grey-shaded area indicates an assumed 30% uncertainty of the total of UNFCCC and natural emissions. Colored symbols represent the various top-down estimates, according to the legend below.

3.3 Comparison with other studies

3.3.1 Comparison of national and European estimates with UNFCCC values

Average a posteriori emissions and their ranges from scenarios S1–S9 are compiled in Table 1 (together with both a priori and UNFCCC emissions). For comparison of a posteriori emissions with UNFCCC values it is important to keep in mind that inverse modelling provides estimates of total emissions, i.e. anthropogenic and natural emissions (including soil sink), while UNFCCC covers the anthropogenic sources only. For most EU-15 countries except Sweden and Finland, however, natural sources contribute only a small fraction of total emissions. The anthropogenic part of the a priori bottom-up inventory used in our study differs from UNFCCC values by up to 30–50% for several European countries (see Table 1), including the 3 largest EU-15 CH_4 emitters Germany, France, and UK. All inversion scenarios presented here (S1–S9) are increasing the CH_4 emissions of these 3 countries compared to our a priori estimate. Assuming that this increase is due to anthropogenic emissions only (i.e. subtracting the small a priori natural sources/sinks from the a posteriori total emissions), this would imply distinctly higher anthropogenic CH_4 emission compared to UNFCCC values (EEA, 2003) (Germany: 3.9 Tg CH_4/yr (+62% compared to EEA (2003)), France: 4.5 Tg CH_4/yr (+47%), and UK: 4.2 Tg CH_4/yr (+93%), based on average values for scenarios S1–S9). Recently, however, Germany revised its CH_4 inventory, resulting in an increase of reported CH_4 emissions by ~70% for the whole time series 1990–2001 (EEA, 2004). For year 2001 this update amounts to an increase of 1.64 Tg CH_4/yr (+68.5%) compared to the CH_4 emission reported in EEA (2003) (Table 1). A major reason for the German update of CH_4 emissions are updated values for CH_4 emissions from manure management, which have

increased from 0.21 to 1.31 Tg CH_4/yr (UBA, 2004). This update of the German inventory leads to a very close agreement with the inverse modelling based values (Table 1). We note, however, that there are still some discrepancies regarding the emissions per source category compared to our a priori emission inventory for Germany. While our bottom-up inventory assumes relatively low CH_4 emissions from manure management (0.26 Tg CH_4/yr) it suggests much higher emissions in particular for landfill sites (1.1 Tg CH_4/yr, compared to 0.50 Tg CH_4/yr (EEA, 2003) and 0.62 Tg CH_4/yr (EEA, 2004). In the framework of the annual reporting of national GHG emissions to UNFCCC it is good practice to recalculate historic emissions in order to account for improvements or changes of methodologies. Beside Germany, also some other EU member states have performed recalculations (e.g. Portugal −24%), but with an overall relatively small effect on absolute total CH_4 emissions. The comparison of inverse modelling results with UNFCCC values is also illustrated in Fig. 10 for Germany, UK, France, and BENELUX.

The EU-15 totals derived from the inversion are relatively close to the UNFCCC values. The a priori total of 21.5 Tg CH_4/yr does not change significantly in the inversion (S1–S9 average: 21.5 Tg CH_4/yr). Assuming total natural CH_4 sources for the EU-15 of 3.9 Tg CH_4/yr (from our a priori inventory) this would imply an EU-15 total of anthropogenic CH_4 sources of 17.5 Tg CH_4/yr, compared to UNFCCC values of 15.7 Tg CH_4/yr (EEA, 2003) and 17.0 Tg CH_4/yr (EEA, 2004). However, our results indicate much smaller CH_4 emissions from Finland, and hence a smaller fraction of natural sources for the EU-15 total emissions. Assuming natural EU-15 emissions of 1 Tg CH_4/yr only (and 21.5 Tg CH_4/yr for the total emissions) would imply 20.5 Tg CH_4/yr for the anthropogenic EU-15 emissions, i.e. 30%/21% higher compared to EEA (2003) and EEA (2004), respectively.

3.3.2 Comparison of Finnish estimates with independent bottom-up studies

Minkkinen et al. (2002) estimated the present-day CH_4 emissions from Finnish peatlands to 0.6 Tg CH_4/yr, based on detailed statistical data for 10 different peatland types. Thus, their estimate is consistent with our inverse modelling derived values (total emissions for Finland −0.27... 1.30 Tg CH_4/yr) taking into account a contribution of 0.24–0.26 Tg CH_4/yr form anthropogenic sources. The main reason for the very high value for Finnish wetlands in the Walter et al. (2001a) inventory (∼3 Tg/yr) seems the underlying wetland distribution (Matthews and Fung, 1987). However, recent vegetation maps, such as Corine land cover database (EEA, 2000) and the Global Land Cover 2000 database (Bartholomé and Belward, 2005) indicate much smaller wetland areas for Finland.

3.3.3 Comparison of national and European estimates with other top-down studies

Figure 10 also shows top-down estimates of other studies over the period 1994 to 2001. The studies of Ryall et al. (2001) and Manning et al. (2003, 2004) are based on NAME, a Langrangian particle dispersion model (LPDM), and observations from Mace Head only. Vermeulen et al. (1999) use the Lagrangian back trajectory model COMET, and alternatively observations of Cabauw only (1993–1997), or a set of 4 European sites (Cabauw, Petten (NL), Heidelberg (D), London (UK), 1996). Roemer et al. (2000) use the LOTOS model, an Eulerian 3-D model on the European domain with initial and boundary conditions taken from the global TM3 model, and observations of 4 Dutch sites (Arnhem, Delft, Kollumerwaard, Cabauw) and Mace Head (1994). The studies based on NAME and COMET do not use an a priori emission inventory. However, they used very long integrations periods (1–6 years) and the assumption that over this period emissions per grid cell or source area are constant.

Considering all studies together, the majority of top-down estimates is reasonably close (∼30–50%) to the UNFCCC bottom-up estimates (corrected with our estimate of natural sources and sinks) for the 4 displayed regions (Germany, UK, France, and BENELUX). There are, however also remarkable discrepancies. In particular striking is the fact that in all studies except that of Manning (2004), the sum of all 4 regions (for the study of Vermeulen et al. (1999) only the 3 regions Germany, UK, and BENELUX are available) is distinctly higher than the corresponding sum of EEA (2003) estimates. As we had seen in our study (Sect. 3.2.5, and Fig. 8) the a posteriori emissions show clear negative correlations, leading typically to relatively robust results for sums of adjacent (coupled) regions. Therefore, the observation of higher sums for the 3–4 regions in the above studies is consistent with the higher emissions from Germany, UK, and France derived from our study compared to EEA (2003). With the revision of the German inventory (EEA, 2004), however, the sum of these regions agrees much better for these above studies.

In contrast, the study of Manning (2004) shows slightly smaller sums for these 4 regions (compared to EEA (2003)), with increasing discrepancy if compared to EEA (2004). Apparent also in Manning (2004), however, is the coupling of these regions (i.e. considerable year-to-year variations for individual countries, but relatively constant sums for all 4 regions).

Model-independent top-down estimates can also be provided using ^{222}Rn measurements. Applying this technique, Levin et al. (1999) derive a mean CH_4 emission of 0.24 ± 0.50 g CH_4 km^{-2} s^{-1} for a catchment area with radius of ∼150 km around Heidelberg for 1995–1997. For a similar catchment area we obtain a mean CH_4 emission of 0.36 ± 0.24 g CH_4 km^{-2} s^{-1} (scenario S1). We note however, that this comparison is problematic because the ^{222}Rn

derived value may be biased towards dominant wind directions (and emissions show considerable variability on small scales, e.g. between $1^\circ \times 1^\circ$ grid boxes). Furthermore, the applied synthesis inversion does not optimize the spatial emission distribution within the predefined regions.

4 Conclusions

The presented analysis provides a consistent picture of the European and global 3-D distribution of atmospheric methane. For most sites an overall good agreement with observations is achieved, including the simulation of synoptic events arising from the short-term ($\sim$1–5 days) variability of meteorological situations.

The atmospheric CH_4 signal has been attributed directly to recent emissions of different European and global regions, on top of a global background (which is also evolving dynamically in space and time).

In particular quasi-continuous observations close to source regions provide significant constraints on the emissions. Largely driven by such high-frequency observations at several Western European sites, the inversion suggests higher emissions for Germany (+62%), France (+47%), and UK (+93%) in 2001 compared to UNFCCC values (EEA, 2003), while results for BENELUX are virtually identical with UNFCCC. The recent revision of the German CH_4 inventory (EEA, 2004), however, leads to a very close agreement with our top-down estimate for Germany.

The question of whether derived higher emissions are really significantly different from UNFCCC values comes down to an exact quantification of uncertainties, which is very difficult, both for the bottom-up and the top-down estimates. Only some EU-15 countries specify uncertainties of their CH_4 estimates, ranging from 1.8% (Sweden) to 48.3% (Austria) (Gugele et al., 2003). No uncertainty estimates are available for the major source countries France and Germany. However, the recent revision of the German CH_4 inventory by $+\sim$70% shows that bottom-up CH_4 inventories may still have considerable uncertainties.

Our inversion suggests significantly lower emissions for Finland, for which the bottom-up inventory had predicted high emissions from wetlands ($\sim$3 Tg CH_4/yr). This finding has been further supported by forward simulations and comparison with observations at Pallas for year 2002. Furthermore, this is consistent with the recent independent estimate of CH_4 emissions from Finnish peatlands of only 0.6 Tg CH_4/yr by Minkkinen et al. (2002).

Significant anti-correlations are apparent between different European regions. Thus despite some remaining uncertainty about the exact distribution among countries, the top-down estimate for total EU-15 emissions appears relatively robust. Furthermore, the derived EU-15 emissions (21.5 Tg CH_4/yr total emissions) are very close to the UNFCCC value for the year 2001 (15.7 Tg CH_4/yr (EEA, 2003); 17.0 Tg CH_4/yr (EEA, 2004)), if the natural net emissions are around 3.9 Tg CH_4/yr, as assumed in our a priori inventory. However, if the fraction of natural emissions is smaller, as our results suggest, our top-down based anthropogenic emission estimate for EU-15 would be 30%/21% higher compared to EEA (2003) and EEA (2004), respectively.

The potential discrepancies between bottom-up and top-down estimates further emphasize the need for independent verification. In a strict sense, however, our top-down approach is not completely independent, as it is using bottom-up inventories as a priori constraints (hence influencing both the model bases functions (emission distribution within one region) and the cost function). Although some other top-down studies based on Lagrangian models avoid the use of a priori inventories, it is noted that the alternative assumptions required (as constant emissions per grid cell or source area over longer integration times) constitute another form of a priori constraint (in these studies implemented as hard constraint; i.e. they cannot be modified by the inverse system). In general the introduction of some a priori constraints is always required due to the underdetermined nature of the overall inverse problem.

Concerning potential implications regarding the targets set by the Kyoto protocol, it is noted that the reduction targets are generally defined relative to the base year 1990, and not in terms of absolute emissions. Consequently, higher absolute emissions of individual countries would not constitute a violation of Kyoto obligations, but only if emissions relative to year 1990 exceed the targets. It is expected that inverse modelling may provide in the future estimates of emission trends with a much smaller uncertainty compared to estimates of absolute emissions as many potential systematic errors remain the same for subsequent years (Dentener et al., 2003b). Nevertheless it still needs to be demonstrated, whether inverse modelling estimates will become accurate enough for verification of the (relatively small) reduction targets.

Our analysis included a discussion of potential systematic errors. In particular, we showed several sensitivity experiments illustrating that a posteriori results are dependent on the exact set of sites used, the data selection procedures and the choice of weighting factors for observations. Regarding the scaling of the OH sink the inversion results for Europe turned out to be very robust.

All the scenarios shown here confirm the major conclusions of this study (including scenario S7, which can be considered as most conservative in the sense that observations are weighted weakly and European sites, with strong regional influence, are not used).

Inverse techniques are a very powerful system analysis tool, allowing to directly link atmospheric observations to emissions. Progress is expected from the further development of inversion techniques including sophisticated data assimilation methods. Furthermore, ensemble inversions applying different models will be particularly useful, in order

to increase the confidence in top-down emission estimates. Additional measurements such as ^{222}Rn and meteorology at all sites would be helpful in order to better assess the ability of the model to simulate the individual sites.

For an operational emission verification system, however, it is particularly important that atmospheric observations are further expanded, especially quasi-continuous high-precision in-situ measurements at well selected sites (Bergamaschi et al., 2004).

Atmospheric CH_4 can now also be measured from satellite-based sensors such as SCIAMACHY on ENVISAT (Buchwitz et al., 2005; Frankenberg et al., 2005), providing a valuable complement to the still rather sparse in-situ measurement network. It is expected that these global observations will provide strong additional constraints in future inverse modelling studies.

Acknowledgements. We thank H. Sartorius for provision of ^{222}Rn measurements at Schauinsland, and K. Uhse and L. Ries for CH_4 data from the German Umweltbundesamt network. Furthermore, we are grateful to ECMWF for the possibility to use their meteorological analyses and A. Segers for his assistance in preprocessing the ECMWF meteo data as TM5 input. We thank M. Amann for provision of IIASA CH_4 bottom-up inventories and B. Gugele for discussion on CH_4 emissions reported to UNFCCC.

Furthermore, we thank T. Alto, F. Raes, A. Leip, J. Wilson, H. Behrend, and I. Levin for helpful comments on the manuscript and S. Houweling for the very helpful review of the ACPD paper.

Edited by: M. Heimann

References

Bartholomé, E., and Belward, A. S.: GLC2000: a new approach to global land cover mapping from Earth Observation data, International Journal of Remote Sensing, in press, 2005.

Bergamaschi, P., Behrend, H., and Jol, A. (Eds.): Inverse modelling of national and EU greenhouse gas emission inventories – report of the workshop "Inverse modelling for potential verification of national and EU bottom-up GHG inventories" under the mandate of the Monitoring Mechanism Committee WG-1 23–24 October 2003, JRC, Ispra, 144, EUR 21099 EN/ISBN 92-894-7455-6, European Commission Joint Research Centre, Ispra, 2004.

Bergamaschi, P., Bräunlich, M., Marik, T., and Brenninkmeijer, C. A. M.: Measurements of the carbon and hydrogen isotopes of atmospheric methane at Izana, Tenerife: Seasonal cycles and synoptic-scale variations, J. Geophys. Res., 105(D11), 14 531–14 546, 2000.

Berkvens, P. J. F., Botchev, M. A., Lioen, W. M., and Verwer, J. G.: A zooming technique for wind transport of air pollution, 31, Centrum voor Wiskunde en Informatica, 1999.

Bousquet, P., Ciais, P., Peylin, P., Ramonet, M., and Monfray, P.: Inverse modeling of annual atmospheric CO_2 sources and sinks: 1. Method and control inversion, J. Geophys. Res., 104(D21), 26 161–26 178, 1999a.

Bousquet, P., Peylin, P., Ciais, P., Ramonet, M., and Monfray, P.: Inverse modeling of annual atmospheric CO_2 sources and sinks: 2. Sensitivity study, J. Geophys. Res., 104(D21), 26 179–26 193, 1999b.

Bouttier, F. and Courtier, P.: Data assimilation concepts and methods, ECMWF, Reading, 1999.

Brühl, C. and Crutzen, P. J.: The MPIC 2D model, in: NASA Ref. Publ. 1292, 1, 103–104, 1993.

Buchwitz, M., de Beek, R., Noël, S., Burrows, J. P., Bovensmann, H., Bremer, H., Bergamaschi, P., Körner, S., Heimann, M.: Carbon monoxide, methane and carbon dioxide columns retrieved from SCIAMACHY by WFM-DOAS: year 2003 initial data set, Atmos. Chem. Phys. Discuss., 5, 1943–1971, 2005, **SRef-ID: 1680-7375/acpd/2005-5-1943**.

Dentener, F., Peters, W., Krol, M., van Weele, M., Bergamaschi, P., and Lelieveld, J.: Inter-annual-variability and trend of CH_4 lifetime as a measure for OH changes in the 1979–1993 time period, J. Geophys. Res., 108(D15), 4442, doi:10.1029/2002JD002916, 2003a.

Dentener, F., van Weele, M., Krol, M., Houweling, S., and van Velthoven, P.: Trends and inter-annual variability of methane emissions derived from 1979–1993 global CTM simulations, Atmos. Chem. Phys., 3, 73–88, 2003b, **SRef-ID: 1680-7324/acp/2003-3-73**.

Dlugokencky, E. J., Steele, L. P., Lang, P. M., and Masarie, K. A.: The growth rate and distribution of atmospheric methane, J. Geophys. Res., 99, 17 021–17 043, 1994.

Dlugokencky, E. J., Steele, L. P., Lang, P. M., and Masarie, K. A.: Atmospheric methane at Mauna Loa and Barrow observatories: Presentation and analysis of in situ measurements, J. Geophys. Res., 100, 23 103–23 113, 1995.

Dlugokencky, E. J., Houweling, S., Bruhwiler, L., Masarie, K. A., Lang, P. M., Miller, J. B., and Tans, P. P.: Atmospheric methane levels off: Temporary pause or a new steady-state?, Geophys. Res. Lett., 30(19), 1992, doi:10.1029/2003GL018126, 2003.

ECMWF, IFS documentation, http://www.ecmwf.int/research/ifsdocs/, 2002.

EEA: Global Land Cover 2000; Version 12/2000 extended coverage; http://dataservice.eea.eu.int/dataservice/metadetails.asp?id=571, European Environment Agency, 2000.

EEA: Annual European Community greenhouse gas inventory 1990–2001 and inventory report 2003, European Environment Agency, Copenhagen, 2003.

EEA: Annual European Community greenhouse gas inventory 1990–2002 and inventory report 2004, European Environment Agency, Copenhagen, 2004.

Engelen, R.: COCO – Measuring CO_2 from space exploiting planned missions 2001–2004, in: Inverse modelling of national and EU greenhouse gas emission inventories – report of the workshop "Inverse modelling for potential verification of national and EU bottom-up GHG inventories" under the mandate of Monitoring Mechanism Committee WG-1 23–24 October 2003, JRC Ispra, EUR 21099 EN/ISBN 92-894-7455-6, edited by: Bergamaschi, P., Behrend, H., and Jol, A., 59–64, European Commission Joint Research Centre, Ispra, 2004.

Enting, I. G.: Green's function methods of tracer inversion, in: Inverse methods in global biogeochemical cycles, edited by: Kasibhatla, P., Heimann, M., Rayner, P., Mahowald, N., Prinn, R. G., and Hartley, D. E., 19–31, American Geophysical Union, Washington D.C., 2000.

Frankenberg, C., Meirink, J. F., van Weele, M., Platt, U., and Wagner, T.: Assessing Methane Emissions from Global Space-Borne Observations, Science, 308, 1010–1014, 2005.

Fung, I., John, J., Lerner, J., Matthews, E., Prather, M., Steele, L. P., and Fraser, P. J.: Three-dimensional model synthesis of the global methane cycle, J. Geophys. Res., 96, 13 033–13 065, 1991.

Goede, A. P. H., Meirink, J. F., Eskes, H., van Weele, M., Burrows, J. P., Buchwitz, M., Monks, P. S., Remeios, J. J., Corlett, G. K., Platt, U., Wagner, T., Stordal, F., Pacyna, J. M., Aben, I., Heimann, M., De Maziere, M., Muller, J.-F., Granier, C., Meyrahn, H., Zander, R., and Bergamaschi, P.: Global Satellite Observation of Greenhouse Gas Emissions – EVERGREEN, in: 34th COSPAR Scientific Assembly, Houston, 2002.

Gugele, B., Huttunen, K., and Ritter, M.: Annual European Community greenhouse gas inventory 1990–2001 and inventory report 2003, European Environment Agency, Copenhagen, 2003.

Gurney, K. R., Law, R. M., Denning, A. S., Rayner, P. J., Baker, D., Bousquet, P., Bruhwiler, L., Chen, Y. H., Ciais, P., Fan, S.-M., Fung, I. Y., Gloor, M., Heimann, M., Higuchi, K., John, J., Makl, T., Maksyutov, S., Masarie, K., Peylin, P., Prather, M., Pak, B. C., Randerson, J., Sarmiento, J., Taguchi, S., Takahashi, T., and Yuen, C.-W.: Towards robust regional estimates of CO2 sources and sinks using atmospheric transport models, Nature, 415, 626–630, 2002.

Heimann, M. and Kaminski, T.: Inverse modeling approaches to infer surface trace gas fluxes from observed atmospheric mixing ratios, Approaches to scaling of trace gas fluxes in ecosystems, in: Approaches to scaling of trace gas fluxes in ecosystems, edited by: Bouwman, A. F., 275–295, Elsevier, Amsterdam, 1999.

Hein, R., Crutzen, P. J., and Heimann, M.: An inverse modeling approach to investigate the global atmospheric methane cycle, Global Biogeochem. Cycles, 11, 43–76, 1997.

Holtslag, A. A. M. and Moeng, C.-H.: Eddy diffusivity and countergradient transport in the convective atmospheric boundary layer, J. Atmos. Sci., 48, 1690–1698, 1991.

Houweling, S., Dentener, F., and Lelieveld, J.: The impact of nonmethane hydrocarbon compounds on tropospheric photochemistry, J. Geophys. Res., 103(D9), 10 673–10 696, 1998.

Houweling, S., Kaminski, T., Dentener, F., Lelieveld, J., and Heimann, M.: Inverse modeling of methane sources and sinks using the adjoint of a global transport model, J. Geophys. Res., 104(D21), 26 137–26 160, 1999.

Houweling, S., Dentener, F. J., and Lelieveld, J.: Simulation of preindustrial atmospheric methane to constrain the global source strength of natural wetlands, J. Geophys. Res., 105, 17 243–17 255, 2000.

IPCC: Revised 1996 IPCC Guidelines for National Greenhouse Gas Inventories, http://www.ipcc-nggip.iges.or.jp/public/gl/invs1.htm, 1996.

IPCC: Good Practice Guidance and Uncertainty Management in National Greenhouse Gas Inventories, 2000.

IPCC: Climate Change 2001: The scientific basis, Cambridge University Press, 2001.

Kaminski, T., Heimann, M., and Giering, T.: A coarse grid three dimensional global inverse model of the atmospheric transport, 1, Adjoint Model and Jacobian Matrix, J. Geophys. Res., 104(D15), 18 535–18 553, 1999a.

Kaminski, T., Heimann, M., and Giering, T.: A coarse grid three-dimensional global inverse model of the atmospheric transport, 2, Inversion of the transport of CO_2 in the 1980s, J. Geophys. Res., 104(D15), 18 555–18 581, 1999b.

Kaminski, T., Rayner, P. J., Heimann, M., and Enting, I. G.: On aggregation errors in atmospheric transport inversions, J. Geophys. Res., 106(D5), 4703–4715, 2001.

Klaassen, G., Amann, M., Berglund, C., Cofala, J., Hoeglund-Isaksson, L., Heyes, C., Mechler, R., Tohka, A., Schoepp, W., and Winiwarter, W.: The extension of the RAINS model to greenhouse gases, 134, International Institute for Applied System Analysis, Laxenburg, 2004.

Krol, M. C., Lelieveld, J., Oram, D. E., Sturrock, G. A., Penkett, S. A., Brenninkmeijer, C. A. M., Gros, V., Williams, J., and Scheeren, H. A.: Continuing emissions of methyl chloroform from Europe, Nature, 421, 131–135, 2003.

Krol, M. C., Houweling, S., Bregman, B., van den Broek, M., Segers, A., van Velthoven, P., Peters, W., Dentener, F., and Bergamaschi, P.: The two-way nested global chemistry-transport zoom model TM5: algorithm and applications, Atmos. Chem. Phys., 5, 417–432, 2005,
SRef-ID: 1680-7324/acp/2005-5-417.

Lelieveld, J., Crutzen, P. J., and Dentener, F. J.: Changing concentration, lifetime and climate forcing of atmospheric methane, Tellus B, 50, 128–150, 1998.

Levin, I., Glatzel-Mattheier, H., Marik, T., Cuntz, M., and Schmidt, M.: Verification of German methane emission inventories and their recent changes based on atmospheric observations, J. Geophys. Res., 104(D3), 3447–3456, 1999.

Li, Y.-F.: Global population distribution (1990), Terrestrial area and country name information on a one by one degree grid cell basis, http://cdiac.ornl.gov/ftp/db1016/, CDIAC, 1996.

Louis, J. F.: A parametric model of vertical eddy fluxes in the atmosphere, Boundary Layer Meteorology, 17, 187–202, 1979.

Manning, A. J.: Estimating European emissions of greenhouse gases, in: Inverse modelling of national and EU greenhouse gas emission inventories – report of the workshop "Inverse modelling for potential verification of national and EU bottom-up GHG inventories" under the mandate of Monitoring Mechanism Committee WG-1 23–24 October 2003, JRC Ispra, EUR 21099 EN/ISBN 92-894-7455-6, edited by: Bergamaschi, P., Behrend, H., and Jol, A., European Commission Joint Research Centre, Ispra, 2004.

Manning, A. J., Ryall, D. B., Derwent, R. G., Simmonds, P. G., and O'Doherty, S.: Estimating European emissions of ozone-depleting and greenhouse gases using observations and a modeling back-attribution technique, J. Geophys. Res., 108(D14), 4405, doi:10.1029/2002JD002312, 2003.

Matthews, E., and Fung, I.: Methane emissions from natural wetlands: Global distribution, area, and environmental characteristics of sources, Global Biogeochem. Cycles, 1, 61–86, 1987.

Matthews, E., Fung, I., and Lerner, J.: Methane emission from rice cultivation: Geographic and seasonal distribution of cultivated areas and emissions, Global Biogeochem. Cycles, 5, 3–24, 1991.

Meirink, J. F., Goede, A., and Partners, E.: EVERGREEN – Global satellite observations of greenhouse gas emissions, in: Inverse modelling of national and EU greenhouse gas emission inventories – report of the workshop "Inverse modelling for potential verification of national and EU bottom-up GHG inventories"

under the mandate of Monitoring Mechanism Committee WG-1 23–24 October 2003, JRC Ispra, EUR 21099 EN/ISBN 92-894-7455-6, edited by: Bergamaschi, P., Behrend, H., and Jol, A., 37–40, European Commission Joint Research Centre, Ispra, 2004.

Mikaloff Fletcher, S. E., Tans, P. P., Bruhwiler, L. M., Miller, J. B., and Heimann, M.: CH_4 sources estimated from atmospheric observations of CH_4 and its $^{13}C/^{12}C$ isotopic ratios: 1. Inverse modelling of source processes, Global Biogeochem. Cycles, 18, doi:10.1029/2004GB002223, 2004a.

Mikaloff Fletcher, S. E., Tans, P. P., Bruhwiler, L. M., Miller, J. B., and Heimann, M.: CH_4 sources estimated from atmospheric observations of CH_4 and its $^{13}C/^{12}C$ isotopic ratios: 2. Inverse modelling of CH_4 fluxes from geographical regions, Global Biogeochem. Cycles, 18, doi:10.1029/2004GB002224, 2004b.

Minkkinen, K., Korhonen, R., and Savolainen, I.: Carbon balance and radiative forcing of Finnish peatlands 1900–2100 – the impact of forestry drainage, Global Change Biology, 8, 785–799, 2002.

Olivier, J. G. J. and Berdowski, J. J. M.: Global emissions sources and sinks, in: The climate system, edited by: Berdowski, J. J. M., Guicherit, R., Heij, B. J., and Balkema, A. A., Publishers/Swets & Zeitlinger Publishers, Lisse, The Netherlands, 2001.

Peters, W., Krol, M. C., Bruhwiler, L., Dlugokencky, E. J., Dutton, G., Miller, J. B., Bergamaschi, P., Dentener, F. J., van Velthoven, P., and Tans, P. P.: Towards regional scale inversion using a two-way nested global model: Characterization of transport using SF_6, J. Geophys. Res., 109, doi:10.1029/2004JD005020, 2004.

Prinn, R., Cunnold, D., Rasmussen, R., Simmonds, P., Alyea, F., Crawford, A., Fraser, P., and Rosen, R.: Atmospheric Emissions and Trends of Nitrous Oxide Deduced From 10 Years of ALE-GAGE Data, J. Geophys. Res., 95(D11), 18 369–18 385, 1990.

Prinn, R. G., Weiss, R. F., Fraser, P. J., Simmonds, P. G., Cunnold, D. M., Alyea, F. N., O'Doherty, S., Salameh, P., Miller, B. R., Huang, J., Wang, R. H. J., Hartley, D. E., Harth, C., Steele, L. P., Sturrock, G., Midgely, P. M., and McCulloch, A.: A history of chemically and radiatively important gases in air deduced from ALE/GAGE/AGAGE, J. Geophys. Res., 115, 17 751–17 792, 2000.

Rödenbeck, C., Houweling, S., Gloor, M., and Heimann, M.: CO_2 flux history 1982–2001 inferred from atmospheric data using a global inversion of atmospheric transport, Atmos. Chem. Phys., 3, 1919–1964, 2003,
SRef-ID: 1680-7324/acp/2003-3-1919.

Roemer, M., van Loon, M., and Boersen, G.: Methane emission verification on a national scale, TNO, Apeldoorn, The Netherlands, 2000.

Russell, G. L. and Lerner, J. A.: A new finite-differencing scheme for the tracer transport equation, J. Appl. Meteor., 20, 1483–1498, 1981.

Ryall, D. B., Derwent, R. G., Manning, A. J., Simmonds, P. G., and O'Doherty, S.: Estimating source regions of European emissions of trace gases from observations at Mace Head, Atmos. Environ., 35, 2507–2523, 2001.

Tarantola, A. and Valette, B.: Generalized nonlinear inverse problems solved using the least square criterion, Rev. Geophys. Space Phys., 20, 219–232, 1982.

Tiedtke, M.: A comprehensive mass flux scheme for cumulus parameterization in large-scale models, Monthly Weather Review, 117, 1779–1800, 1987.

UBA: Deutsches Treibhausgasinventar 1990–2002: Nationaler Inventarbericht 2004 – Berichterstattung unter der Klimarahmenkonvention der Vereinten Nationen, pp. 398 pp, Umweltbundesamt, Berlin, 2004.

Vermeulen, A., Eisma, R., Hensen, A., and Slanina, J.: Transport model calculations of NW European methane emissions, Env. Sci. & Policy, 2, 315–324, 1999.

Walter, B. P. and Heimann, M.: A process-based, climate-sensitive model to derive methane emissions from natural wetlands: Application to five wetland sites, sensitivity to model parameters, and climate, Global Biogeochem. Cycles, 14, 3, 745–765, 2000.

Walter, B. P., Heimann, M., and Matthews, E.: Modeling modern methane emissions from natural wetlands 1. Model description and results, J. Geophys. Res., 106, 34 189–34 206, 2001a.

Walter, B. P., Heimann, M., and Matthews, E.: Modeling modern methane emissions from natural wetlands 2. Interannual variations 1982–1993, J. Geophys. Res., 106, 34 207–34 217, 2001b.

WMO: Global Atmospheric Watch World Data Centre for Greenhouse Gases, 92, Japan Meteorological Agency in co-operation with World Meteorological Organisation, 2003.